9. QUANTUM CHROMODYNAMICS

Written October 2009 by G. Dissertori (ETH, Zurich) and G.P. Salam (LPTHE, Paris).

9.1. Basics

Quantum Chromodynamics (QCD), the gauge field theory that describes the strong interactions of colored quarks and gluons, is the SU(3) component of the SU(3)×SU(2)×U(1) Standard Model of Particle Physics.

The Lagrangian of QCD is given by

$$\mathcal{L} = \sum_q \bar{\psi}_{q,a}(i\gamma^\mu \partial_\mu \delta_{ab} - g_s \gamma^\mu t^C_{ab} \mathcal{A}^C_\mu - m_q \delta_{ab})\psi_{q,b} - \frac{1}{4} F^A_{\mu\nu} F^{A\,\mu\nu}\,, \tag{9.1}$$

where repeated indices are summed over. The γ^μ are the Dirac γ-matrices. The $\psi_{q,a}$ are quark-field spinors for a quark of flavor q and mass m_q, with a color-index a that runs from $a = 1$ to $N_c = 3$, *i.e.* quarks come in three "colors." Quarks are said to be in the fundamental representation of the SU(3) color group.

The $\mathcal{A}^C_\mu$ correspond to the gluon fields, with C running from 1 to $N_c^2 - 1 = 8$, *i.e.* there are eight kinds of gluon. Gluons are said to be in the adjoint representation of the SU(3) color group. The t^C_{ab} correspond to eight 3×3 matrices and are the generators of the SU(3) group (cf. the section on "SU(3) isoscalar factors and representation matrices" in this *Review* with $t^C_{ab} \equiv \lambda^C_{ab}/2$). They encode the fact that a gluon's interaction with a quark rotates the quark's color in SU(3) space. The quantity g_s is the QCD coupling constant. Finally, the field tensor $F^A_{\mu\nu}$ is given by

$$F^A_{\mu\nu} = \partial_\mu \mathcal{A}^A_\nu - \partial_\nu \mathcal{A}^A_\mu - g_s\, f_{ABC} \mathcal{A}^B_\mu \mathcal{A}^C_\nu \qquad [t^A, t^B] = i f_{ABC} t^C\,, \tag{9.2}$$

where the f_{ABC} are the structure constants of the SU(3) group.

Neither quarks nor gluons are observed as free particles. Hadrons are color-singlet (*i.e.* color-neutral) combinations of quarks, anti-quarks, and gluons.

Ab-initio predictive methods for QCD include lattice gauge theory and perturbative expansions in the coupling. The Feynman rules of QCD involve a quark-antiquark-gluon ($q\bar{q}g$) vertex, a 3-gluon vertex (both proportional to g_s), and a 4-gluon vertex (proportional to g_s^2). A full set of Feynman rules is to be found for example in Ref. 1.

Useful color-algebra relations include: $t^A_{ab} t^A_{bc} = C_F \delta_{ac}$, where $C_F \equiv (N_c^2 - 1)/(2N_c) = 4/3$ is the color-factor ("Casimir") associated with gluon emission from a quark; $f^{ACD} f^{BCD} = C_A \delta_{AB}$ where $C_A \equiv N_c = 3$ is the color-factor associated with gluon emission from a gluon; $t^A_{ab} t^B_{ab} = T_R \delta_{AB}$, where $T_R = 1/2$ is the color-factor for a gluon to split to a $q\bar{q}$ pair.

The fundamental parameters of QCD are the coupling g_s (or $\alpha_s = \dfrac{g_s^2}{4\pi}$) and the quark masses m_q.

This review will concentrate mainly on perturbative aspects of QCD as they relate to collider physics. Related textbooks include Refs. 1–3. Some discussion of non-perturbative aspects, including lattice QCD, is to be found in the reviews on "Quark Masses" and "The CKM quark-mixing matrix" of this *Review*. Lattice-QCD textbooks and lecture notes include Refs. 4–6, while recent developments are summarized for example in Ref. 7. For a review of some of the QCD issues in heavy-ion physics, see for example Ref. 8.

9.1.1. *Running coupling* :

In the framework of perturbative QCD (pQCD), predictions for observables are expressed in terms of the renormalized coupling $\alpha_s(\mu_R^2)$, a function of an (unphysical) renormalization scale μ_R. When one takes μ_R close to the scale of the momentum transfer Q in a given process, then $\alpha_s(\mu_R^2 \simeq Q^2)$ is indicative of the effective strength of the strong interaction in that process.

The coupling satisfies the following renormalization group equation (RGE):

$$\mu_R^2 \frac{d\alpha_s}{d\mu_R^2} = \beta(\alpha_s) = -(b_0\alpha_s^2 + b_1\alpha_s^3 + b_2\alpha_s^4 + \cdots) \tag{9.3}$$

where $b_0 = (11C_A - 4n_f T_R)/(12\pi) = (33 - 2n_f)/(12\pi)$ is referred to as the 1-loop beta-function coefficient, the 2-loop coefficient is $b_1 = (17C_A^2 - n_f T_R(10C_A + 6C_F))/(24\pi^2) = (153 - 19n_f)/(24\pi^2)$, and the 3-loop coefficient is $b_2 = (2857 - \frac{5033}{9}n_f + \frac{325}{27}n_f^2)/(128\pi^3)$. The 4-loop coefficient, b_3, is to be found in Refs. 9, 10†. The minus sign in Eq. (9.3) is the origin of asymptotic freedom, *i.e.* the fact that the strong coupling becomes weak for processes involving large momentum transfers ("hard processes"), $\alpha_s \sim 0.1$ for momentum transfers in the 100 GeV –TeV range.

The β-function coefficients, the b_i, are given for the coupling of an *effective theory* in which n_f of the quark flavors are considered light ($m_q \ll \mu_R$), and in which the remaining heavier quark flavors decouple from the theory. One may relate the coupling for the theory with $n_f + 1$ light flavors to that with n_f flavors through an equation of the form

$$\alpha_s^{(n_f+1)}(\mu_R^2) = \alpha_s^{(n_f)}(\mu_R^2)\left(1 + \sum_{n=1}^{\infty}\sum_{\ell=0}^{n} c_{n\ell}\,[\alpha_s^{(n_f)}(\mu_R^2)]^n \ln^\ell \frac{\mu_R^2}{m_h^2}\right), \tag{9.4}$$

where m_h is the mass of the $(n_f+1)^{\text{th}}$ flavor, and the first few $c_{n\ell}$ coefficients are $c_{11} = \frac{1}{6\pi}$, $c_{10} = 0$, $c_{22} = c_{11}^2$, $c_{21} = \frac{19}{24\pi^2}$, and $c_{20} = -\frac{11}{72\pi^2}$ when m_h is the $\overline{\text{MS}}$ mass at scale m_h ($c_{20} = \frac{7}{24\pi^2}$ when m_h is the pole mass — mass definitions are discussed below and in the review on "Quark Masses"). Terms up to $c_{4\ell}$ are to be found in Refs. 11, 12. Numerically, when one chooses $\mu_R = m_h$, the matching is a small effect, owing to the zero value for the c_{10} coefficient.

† One should be aware that the b_2 and b_3 coefficients are renormalization-scheme-dependent, and given here in the $\overline{\text{MS}}$ scheme, as discussed below.

Working in an energy range where the number of flavors is constant, a simple exact analytic solution exists for Eq. (9.3) only if one neglects all but the b_0 term, giving $\alpha_s(\mu_R^2) = (b_0 \ln(\mu_R^2/\Lambda^2))^{-1}$. Here Λ is a constant of integration, which corresponds to the scale where the perturbatively-defined coupling would diverge, *i.e.* it is the non-perturbative scale of QCD. A convenient approximate analytic solution to the RGE that includes also the b_1, b_2, and b_3 terms is given by (see for example Ref. 13),

$$\alpha_s(\mu_R^2) \simeq \frac{1}{b_0 t}\left(1 - \frac{b_1}{b_0^2}\frac{\ln t}{t} + \frac{b_1^2(\ln^2 t - \ln t - 1) + b_0 b_2}{b_0^4 t^2}\right.$$

$$\left. - \frac{b_1^3(\ln^3 t - \frac{5}{2}\ln^2 t - 2\ln t + \frac{1}{2}) + 3b_0 b_1 b_2 \ln t - \frac{1}{2}b_0^2 b_3}{b_0^6 t^3}\right), \quad t \equiv \ln\frac{\mu_R^2}{\Lambda^2}\,, \qquad (9.5)$$

again parametrized in terms of a constant Λ. Note that Eq. (9.5) is one of several possible approximate 4-loop solutions for $\alpha_s(\mu_R^2)$, and that a value for Λ only defines $\alpha_s(\mu_R^2)$ once one knows which particular approximation is being used. An alternative to the use of formulas such as Eq. (9.5) is to solve the RGE exactly, numerically (including the discontinuities, Eq. (9.4), at flavor thresholds). In such cases the quantity Λ is not defined at all. For these reasons, in determinations of the coupling, it has become standard practice to quote the value of α_s at a given scale (typically M_Z) rather than to quote a value for Λ.

The value of the coupling, as well as the exact forms of the b_2, c_{10} (and higher order) coefficients, depend on the renormalization scheme in which the coupling is defined, *i.e.* the convention used to subtract infinities in the context of renormalization. The coefficients given above hold for a coupling defined in the modified minimal subtraction ($\overline{\rm MS}$) scheme [14], by far the most widely used scheme.

A discussion of determinations of the coupling and a graph illustrating its scale dependence ("running") are to be found in Section 9.3.4.

9.1.2. *Quark masses* :

Free quarks are never observed, *i.e.* a quark never exists on its own for a time longer than $\sim 1/\Lambda$: up, down, strange, charm, and bottom quarks all *hadronize*, *i.e.* become part of a meson or baryon, on a timescale $\sim 1/\Lambda$; the top quark instead decays before it has time to hadronize. This means that the question of what one means by the quark mass is a complex one, which requires that one adopts a specific prescription. A perturbatively defined prescription is the pole mass, m_q, which corresponds to the position of the divergence of the propagator. This is close to one's physical picture of mass. However, when relating it to observable quantities, it suffers from substantial non-perturbative ambiguities (see *e.g.* Ref. 15). An alternative is the $\overline{\rm MS}$ mass, $\overline{m}_q(\mu_R^2)$, which depends on the renormalization scale μ_R.

Results for the masses of heavier quarks are often quoted either as the pole mass or as the $\overline{\rm MS}$ mass evaluated at a scale equal to the mass, $\overline{m}_q(\overline{m}_q^2)$; light quark masses are generally quoted in the $\overline{\rm MS}$ scheme at a scale $\mu_R \sim 2$ GeV . The pole and $\overline{\rm MS}$ masses are

related by a slowly converging series that starts $m_q = \overline{m}_q(\overline{m}_q^2)(1 + \frac{4\alpha_s(\overline{m}_q^2)}{3\pi} + \mathcal{O}(\alpha_s^2))$, while the scale-dependence of $\overline{\rm MS}$ masses is given by

$$\mu_R^2 \frac{d\overline{m}_q(\mu_R^2)}{d\mu_R^2} = \left[-\frac{\alpha_s(\mu_R^2)}{\pi} + \mathcal{O}(\alpha_s^2)\right]\overline{m}_q(\mu_R^2)\,. \tag{9.6}$$

Quark masses are discussed in detail in a dedicated section of the *Review*, "Quark Masses."

9.2. Structure of QCD predictions

9.2.1. *Inclusive cross sections* :

The simplest observables in QCD are those that do not involve initial-state hadrons and that are fully inclusive with respect to details of the final state. One example is the total cross section for $e^+e^- \to$ hadrons at center-of-mass energy Q, for which one can write

$$\frac{\sigma(e^+e^- \to \text{hadrons}, Q)}{\sigma(e^+e^- \to \mu^+\mu^-, Q)} \equiv R(Q) = R_{\rm EW}(Q)(1 + \delta_{\rm QCD}(Q))\,, \tag{9.7}$$

where $R_{\rm EW}(Q)$ is the purely electroweak prediction for the ratio and $\delta_{\rm QCD}(Q)$ is the correction due to QCD effects. To keep the discussion simple, we can restrict our attention to energies $Q \ll M_Z$, where the process is dominated by photon exchange ($R_{\rm EW} = 3\sum_q e_q^2$, neglecting finite-quark-mass corrections),

$$\delta_{\rm QCD}(Q) = \sum_{n=1}^{\infty} c_n \cdot \left(\frac{\alpha_s(Q^2)}{\pi}\right)^n + \mathcal{O}\left(\frac{\Lambda^4}{Q^4}\right)\,. \tag{9.8}$$

The first four terms in the α_s series expansion are then to be found in Refs. 16, 17

$$c_1 = 1\,, \qquad c_2 = 1.9857 - 0.1152 n_f\,, \tag{9.9a}$$

$$c_3 = -6.63694 - 1.20013 n_f - 0.00518 n_f^2 - 1.240\eta \tag{9.9b}$$

$$c_4 = -156.61 + 18.77 n_f - 0.7974 n_f^2 + 0.0215 n_f^3 + C\eta\,, \tag{9.9c}$$

with $\eta = (\sum e_q)^2/(3\sum e_q^2)$ and where the coefficient C of the η-dependent piece in the α_s^4 term has yet to be determined. For corresponding expressions including also Z exchange and finite-quark-mass effects, see Ref. 18.

A related series holds also for the QCD corrections to the hadronic decay width of the τ lepton, which essentially involves an integral of $R(Q)$ over the allowed range of invariant masses of the hadronic part of the τ decay (see e.g. Ref. 16). The series expansions for QCD corrections to Higgs-boson (partial) decay widths are summarized in Refs. 19, 20.

One characteristic feature of the Eq. (9.8) is that the coefficients of α_s^n increase rapidly order by order: calculations in perturbative QCD tend to converge more slowly than

would be expected based just on the size of α_s[††]. Another feature is the existence of an extra "power-correction" term $\mathcal{O}(\Lambda^4/Q^4)$ in Eq. (9.8), which accounts for contributions that are fundamentally non-perturbative. All high-energy QCD predictions involve such corrections, though the exact power of Λ/Q depends on the observable.

Scale dependence. In Eq. (9.8) the renormalization scale for α_s has been chosen equal to Q. The result can also be expressed in terms of the coupling at an arbitrary renormalization scale μ_R,

$$\delta_{\rm QCD}(Q) = \sum_{n=1}^{\infty} \overline{c}_n\left(\frac{\mu_R^2}{Q^2}\right) \cdot \left(\frac{\alpha_s(\mu_R^2)}{\pi}\right)^n + \mathcal{O}\left(\frac{\Lambda^4}{Q^4}\right) , \tag{9.10}$$

where $\overline{c}_1(\mu_R^2/Q^2) \equiv c_1$, $\overline{c}_2(\mu_R^2/Q^2) = c_2 + \pi b_0 c_1 \ln(\mu_R^2/Q^2)$, $\overline{c}_3(\mu_R^2/Q^2) = c_3 + (2b_0c_2\pi + b_1c_1\pi^2)\ln(\mu_R^2/Q^2) + b_0^2c_1\pi^2\ln^2(\mu_R^2/Q^2)$, *etc.*. Given an infinite number of terms in the α_s expansion, the μ_R dependence of the $\overline{c}_n(\mu_R^2/Q^2)$ coefficients will exactly cancel that of $\alpha_s(\mu_R^2)$, and the final result will be independent of the choice of μ_R: physical observables do not depend on unphysical scales.

With just terms up to $n = N$, a residual μ_R dependence will remain, which implies an uncertainty on the prediction of $R(Q)$ due to the arbitrariness of the scale choice. This uncertainty will be $\mathcal{O}(\alpha_s^{N+1})$, *i.e.* of the same order as the neglected terms. For this reason it is standard to use QCD predictions' scale dependence as an estimate of the uncertainties due to neglected terms. One usually takes a central value for $\mu_R \sim Q$, in order to avoid the poor convergence of the perturbative series that results from the large $\ln^{n-1}(\mu_R^2/Q^2)$ terms in the $\overline{c}_n$ coefficients when $\mu_R \ll Q$ or $\mu_R \gg Q$.

9.2.1.1. *Processes with initial-state hadrons:*

Deep Inelastic Scattering. To illustrate the key features of QCD cross sections in processes with initial-state hadrons, let us consider deep-inelastic scattering (DIS), $ep \to e + X$, where an electron e with four-momentum k emits a highly off-shell photon (momentum q) that interacts with the proton (momentum p). For photon virtualities $Q^2 \equiv -q^2$ far above the squared proton mass (but far below the Z mass), the differential cross section in terms of the kinematic variables Q^2, $x = Q^2/(2p\cdot q)$ and $y = (q\cdot p)/(k\cdot p)$ is

$$\frac{d^2\sigma}{dxdQ^2} = \frac{4\pi\alpha}{2xQ^4}\left[(1+(1-y)^2)F_2(x,Q^2) - y^2F_L(x,Q^2)\right] , \tag{9.11}$$

where α is the electromagnetic coupling and $F_2(x,Q^2)$ and $F_L(x,Q^2)$ are proton structure functions, which encode the interaction between the photon (in given polarization states) and the proton (for an extended review, see Sec. 16).

Structure functions are not calculable in perturbative QCD, nor is any other cross section that involves initial-state hadrons. To zeroth order in α_s, the structure functions

[††] The situation is significantly worse near thresholds, e.g. the $t\bar{t}$ production threshold. An overview of some of the "effective field theory" techniques used in such cases is to be found for example in Ref. 21.

are given directly in terms of non-perturbative parton (quark or gluon) distribution functions (PDFs),

$$F_2(x,Q^2) = x\sum_q e_q^2 f_{q/p}(x)\,, \qquad F_L(x,Q^2) = 0\,, \tag{9.12}$$

where $f_{q/p}(x)$ is the PDF for quarks of type q inside the proton, *i.e.* the number density of quarks of type q inside a fast-moving proton that carry a fraction x of its longitudinal momentum (the quark flavor index q, here, is not to be confused with the photon momentum q in the lines preceding Eq. (9.11)). Since PDFs are non-perturbative, and difficult to calculate in lattice QCD [22], they must be extracted from data.

The above result, with PDFs $f_{q/p}(x)$ that are independent of the scale Q, corresponds to the "quark-parton model" picture in which the photon interacts with point-like free quarks, or equivalently, one has incoherent elastic scattering between the electron and individual constituents of the proton. As a consequence, in this picture also F_2 and F_L are independent of Q. When including higher orders in pQCD, Eq. (9.12) becomes

$$\begin{aligned} F_2(x,Q^2) = \\ & x\sum_{n=0}^{\infty}\frac{\alpha_s^n(\mu_R^2)}{(2\pi)^n}\sum_{i=q,g}\int_x^1\frac{dz}{z}C_{2,i}^{(n)}(z,Q^2,\mu_R^2,\mu_F^2)\,f_{i/p}\Big(\frac{x}{z},\mu_F^2\Big) \\ & + \mathcal{O}\Big(\frac{\Lambda^2}{Q^2}\Big)\,. \end{aligned} \tag{9.13}$$

Just as in Eq. (9.10), we have a series in powers $\alpha_s(\mu_R^2)$, each term involving a coefficient $C_{2,i}^{(n)}$ that can be calculated using Feynman graphs. An important difference relative to Eq. (9.10) stems from the fact that the quark's momentum, when it interacts with the photon, can differ from its momentum when it was extracted from the proton, because it may have radiated gluons in between. As a result, the $C_{2,i}^{(n)}$ coefficients are functions that depend on the ratio, z, of these two momenta, and one must integrate over z. At zeroth order, $C_{2,q}^{(0)} = e_q^2\delta(1-z)$ and $C_{2,g}^{(0)} = 0$.

The majority of the emissions that modify a parton's momentum are actually collinear (parallel) to that parton, and don't depend on the fact that the parton is destined to interact with a photon. It is natural to view these emissions as modifying the proton's structure rather than being part of the coefficient function for the parton's interaction with the photon. The separation between the two categories is somewhat arbitrary and parametrized by a *factorization scale*, μ_F. Technically, one uses a procedure known as *factorization* to give rigorous meaning to this distinction, most commonly through the $\overline{\rm MS}$ factorization scheme, defined in the context of dimensional regularization. The $\overline{\rm MS}$ factorization scheme involves an arbitrary choice of *factorization scale*, μ_F, whose meaning can be understood roughly as follows: emissions with transverse momenta above μ_F are included in the $C_{2,q}^{(n)}(z,Q^2,\mu_R^2,\mu_F^2)$; emissions with transverse momenta below μ_F are accounted for within the PDFs, $f_{i/p}(x,\mu_F^2)$.

The PDFs' resulting dependence on μ_F is described by the Dokshitzer-Gribov-Lipatov-Altarelli-Parisi (DGLAP) equations [23], which to leading order (LO) read*

$$\frac{\partial f_{i/p}(x,\mu_F^2)}{\partial \mu_F^2} = \sum_j \frac{\alpha_s(\mu_F^2)}{2\pi} \int_x^1 \frac{dz}{z} P^{(1)}_{i\leftarrow j}(z) f_{j/p}\left(\frac{x}{z},\mu_F^2\right), \tag{9.14}$$

with, for example, $P^{(1)}_{q\leftarrow g}(z) = T_R(z^2+(1-z)^2)$. The other LO splitting functions are listed in Sec. 16 of this *Review*, while results up to next-to-next-to-leading order (NNLO), α_s^3, are given in Refs. 24, 25. The coefficient functions are also μ_F dependent, for example $C^{(1)}_{2,i}(x,Q^2,\mu_R^2,\mu_F^2) = C^{(1)}_{2,i}(x,Q^2,\mu_R^2,Q^2) - \ln(\frac{\mu_F^2}{Q^2}) \sum_j \int_x^1 \frac{dz}{z} P^{(1)}_{i\leftarrow j}(z) C^{(0)}_{2,j}(\frac{x}{z})$. For the electromagnetic component of DIS with light quarks and gluons they are known to $\mathcal{O}(\alpha_s^3)$ (N^{3}LO) [26]. For weak currents they are known fully to α_s^2 (NNLO) [27] with substantial results known also at N^{3}LO [28]. For heavy quark production they are known to $\mathcal{O}(\alpha_s^2)$ [29] (next-to-leading order (NLO) insofar as the series starts at $\mathcal{O}(\alpha_s)$), with work ongoing towards NNLO [30].

As with the renormalization scale, the choice of factorization scale is arbitrary, but if one has an infinite number of terms in the perturbative series, the μ_F-dependences of the coefficient functions and PDFs will compensate each other fully. Given only N terms of the series, a residual uncertainty $\mathcal{O}(\alpha_s^{N+1})$ is associated with the ambiguity in the choice of μ_F. As with μ_R, varying μ_F provides an input in estimating uncertainties on predictions. In inclusive DIS predictions, the default choice for the scales is usually $\mu_R = \mu_F = Q$.

Hadron-hadron collisions. The extension to processes with two initial-state hadrons is straightforward, and for example the total (inclusive) cross section for W boson production in $p\bar{p}$ collisions can be written as

$$\sigma(p\bar{p}\to W+X) = \sum_{n=0}^{\infty} \alpha_s^n(\mu_R^2) \sum_{i,j} \int dx_1 dx_2\, f_{i/p}\Big(x_1,\mu_F^2\Big) f_{j/\bar{p}}\Big(x_2,\mu_F^2\Big) \times \hat{\sigma}^{(n)}_{ij\to W+X}\Big(x_1x_2s,\mu_R^2,\mu_F^2\Big), \tag{9.15}$$

where s is the squared center-of-mass energy of the collision. At LO, $n=0$, the hard (partonic) cross section $\hat{\sigma}^{(0)}_{ij\to W+X}(x_1x_2s,\mu_R^2,\mu_F^2)$ is simply proportional to

* LO is generally taken to mean the lowest order at which a quantity is non-zero. This definition is nearly always unambiguous, the one major exception being for the case of the hadronic branching ratio of virtual photons, Z, τ, etc., for which two conventions exist: LO can either mean the lowest order that contributes to the hadronic branching fraction, *i.e.* the term "1" in Eq. (9.7); or it can mean the lowest order at which the hadronic branching ratio becomes sensitive to the coupling, $n=1$ in Eq. (9.8), as is relevant when extracting the value of the coupling from a measurement of the branching ratio. Because of this ambiguity, we avoided use of the term "LO" in that context.

$\delta(x_1 x_2 s - M_W^2)$, in the narrow W-boson width approximation (see Sec. 40 of this Review for detailed expressions for this and other hard scattering cross sections). It is non-zero only for choices of i, j that can directly give a W, such as $i = u$, $j = \bar{d}$. At higher orders, $n \geq 1$, new partonic channels contribute, such as gq, and there is no restriction $x_1 x_2 s = M_W^2$.

Equation 9.15 involves a factorization between hard cross section and PDFs, just like Eq. (9.13). As long as the same factorization scheme is used in DIS and pp or $p\bar{p}$ (usually the $\overline{\rm MS}$ scheme), then PDFs extracted in DIS can be directly used in pp and $p\bar{p}$ predictions [31].

The fully inclusive hard cross sections are known to NNLO, α_s^2, for Drell-Yan (DY) lepton-pair and vector-boson production [32,33], and for Higgs-boson production [33–36].

Photoproduction. γp (and $\gamma\gamma$) collisions are similar to pp collisions, with the subtlety that the photon can behave in two ways: there is "direct" photoproduction, in which the photon behaves as a point-like particle and takes part directly in the hard collision, with hard subprocesses such as $\gamma g \to q\bar{q}$; there is also resolved photoproduction, in which the photon behaves like a hadron, with non-perturbative partonic substructure and a corresponding PDF for its quark and gluon content, $f_{i/\gamma}(x, Q^2)$.

While useful to understand the general structure of γp collisions, the distinction between direct and resolved photoproduction is not well defined beyond leading order, as discussed for example in Ref. 37.

The high-energy limit. In situations in which the total center-of-mass energy $\sqrt{s}$ is much larger than other scales in the problem (*e.g.* Q in DIS, m_b for $b\bar{b}$ production in pp collisions, *etc.*), each power of α_s beyond LO can be accompanied by a power of $\ln(s/Q^2)$ (or $\ln(s/m_b^2)$, *etc.*). This is known as the high-energy or Balitsky-Fadin-Kuraev-Lipatov (BFKL) limit [38–40]. Currently it is possible to account for the dominant and first subdominant [41,42] power of $\ln s$ at each order of α_s, and also to estimate further subdominant contributions that are numerically large (see Refs. 43–45 and references therein).

Physically, the summation of all orders in α_s can be understood as leading to a growth with s of the gluon density in the proton. At sufficiently high energies this implies non-linear effects, whose treatment has been the subject of intense study (see for example Refs. 46, 47 and references thereto).

9.2.2. *Non-inclusive cross-sections* :

QCD final states always consist of hadrons, while perturbative QCD calculations deal with partons. Physically, an energetic parton fragments ("showers") into many further partons, which then, on later timescales, undergo a transition to hadrons ("hadronization"). Fixed-order perturbation theory captures only a small part of these dynamics.

This does not matter for the fully inclusive cross sections discussed above: the showering and hadronization stages are "unitary", *i.e.* they do not change the overall probability of hard scattering, because they occur long after it has taken place.

Non-inclusive measurements, in contrast, may be affected by the extra dynamics. For those sensitive just to the main directions of energy flow (jet rates, event shapes, cf. Sec. 9.3.1) fixed order perturbation theory is often still adequate, because showering and hadronization don't substantially change the overall energy flow. This means that one can make a prediction using just a small number of partons, which should correspond well to a measurement of the same observable carried out on hadrons. For observables that instead depend on distributions of individual hadrons (which, e.g., are the inputs to detector simulations), it is mandatory to account for showering and hadronization. The range of predictive techniques available for QCD final states reflects this diversity of needs of different measurements.

While illustrating the different methods, we shall for simplicity mainly use expressions that hold for e^+e^- scattering. The extension to cases with initial-state partons will be mostly straightforward (space constraints unfortunately prevent us from addressing diffraction and exclusive hadron-production processes; extensive discussion is to be found in Refs. 48, 49).

9.2.2.1. *Preliminaries: Soft and collinear limits:*

Before examining specific predictive methods, it is useful to be aware of a general property of QCD matrix elements in the soft and collinear limits. Consider a squared tree-level matrix element $|M_n^2(p_1,\ldots,p_n)|$ for the production of n partons with momenta $p_1,\ldots,p_n$, and a corresponding phase-space integration measure $d\Phi_n$. If particle n is a gluon, and additionally it becomes collinear (parallel) to another particle i and its momentum tends to zero (it becomes "soft"), the matrix element simplifies as follows,

$$\lim_{\theta_{in}\to 0,\, E_n\to 0} d\Phi_n |M_n^2(p_1,\ldots,p_n)| \\ = d\Phi_{n-1}|M_{n-1}^2(p_1,\ldots,p_{n-1})| \frac{\alpha_s C_i}{\pi}\frac{d\theta_{in}^2}{\theta_{in}^2}\frac{dE_n}{E_n}\,, \tag{9.16}$$

where $C_i = C_F$ (C_A) if i is a quark (gluon). This formula has non-integrable divergences both for the inter-parton angle $\theta_{in}\to 0$ and for the gluon energy $E_n\to 0$, which are mirrored also in the structure of divergences in loop diagrams. These divergences are important for at least two reasons: firstly, they govern the typical structure of events (inducing many emissions either with low energy or at small angle with respect to hard partons); secondly, they will determine which observables can be calculated within perturbative QCD.

9.2.2.2. *Fixed-order predictions:*

Let us consider an observable $\mathcal{O}$ that is a function $\mathcal{O}_m(p_1,\ldots,p_m)$ of the four-momenta of the m particles in an event (whether partons or hadrons). In what follows, we shall consider the cross section for events weighted with the value of the observable, $\sigma_{\mathcal{O}}$. As examples, if $\mathcal{O}_m \equiv 1$ for all m, then $\sigma_{\mathcal{O}}$ is just the total cross section; if $\mathcal{O}_m \equiv \hat{\tau}(p_1,\ldots,p_m)$ where $\hat{\tau}$ is the value of the thrust for that event (see Sec. 9.3.1.2), then the average value of the thrust is $\langle\tau\rangle = \sigma_{\mathcal{O}}/\sigma_{\rm tot}$; if $\mathcal{O}_m \equiv \delta(\tau - \hat{\tau}(p_1,\ldots,p_m))$ then one gets the differential cross section as a function of the thrust, $\sigma_{\mathcal{O}} \equiv d\sigma/d\tau$.

In the expressions below, we shall omit to write the non-perturbative power correction term, which for most common observables is proportional to a single power of Λ/Q.

LO. If the observable $\mathcal{O}$ is non-zero only for events with at least n particles, then the LO QCD prediction for the weighted cross section in e^+e^- annihilation is

$$\sigma_{\mathcal{O},LO} = \alpha_s^{n-2}(\mu_R^2) \int d\Phi_n |M_n^2(p_1,\ldots,p_n)|\, \mathcal{O}_n(p_1,\ldots,p_n)\,, \tag{9.17}$$

where the squared tree-level matrix element, $|M_n^2(p_1,\ldots,p_n)|$, includes relevant symmetry factors, has been summed over all subprocesses (e.g. $e^+e^- \to q\bar{q}q\bar{q}$, $e^+e^- \to q\bar{q}gg$) and has had all factors of α_s extracted in front. In processes other than e^+e^- collisions, the powers of the coupling are often brought inside the integrals, with the scale μ_R chosen event by event, as a function of the event kinematics.

Other than in the simplest cases (see the review on Cross Sections in this *Review*), the matrix elements in Eq. (9.17) are usually calculated automatically with programs such as CompHEP [50], MadGraph [51], Alpgen [52], Comix/Sherpa [53], and Helac/Phegas [54]. Some of these (CompHEP, MadGraph) use formulae obtained from direct evaluations of Feynman diagrams. Others (Alpgen, Helac/Phegas and Comix/Sherpa) use methods designed to be particularly efficient at high multiplicities, such as Berends-Giele recursion [55] (see also the review Ref. 56), which builds up amplitudes for complex processes from simpler ones.

The phase-space integration is usually carried out by Monte Carlo sampling, in order to deal with the sometimes complicated cuts that are used in corresponding experimental measurements. Because of the divergences in the matrix element, Eq. (9.16), the integral converges only if the observable vanishes for kinematic configurations in which one of the n particles is arbitrarily soft or it is collinear to another particle. As an example, the cross section for producing any configuration of n partons will lead to an infinite integral, whereas a finite result will be obtained for the cross section for producing n deposits of energy (or jets, see Sec. 9.3.1.1), each above some energy threshold and well separated from each other in angle.

LO calculations can be carried out for $2 \to n$ processes with $n \lesssim 6-10$. The exact upper limit depends on the process, the method used to evaluate the matrix elements (recursive methods are more efficient), and the extent to which the phase-space integration can be optimized to work around the large variations in the values of the matrix elements.

NLO. Given an observable that is non-zero starting from n particles, its prediction at NLO involves supplementing the LO result with the $(n+1)$-particle tree-level matrix element ($|M_{n+1}^2|$), and the interference of a n-particle tree-level and n-particle 1-loop amplitude ($2\mathrm{Re}(M_n M^*_{n,1-\mathrm{loop}})$),

$$\begin{aligned}\sigma_{\mathcal{O}}^{NLO} = \sigma_{\mathcal{O}}^{LO} &+ \alpha_s^{n-1}(\mu_R^2) \int d\Phi_{n+1} \\ &|M_{n+1}^2(p_1,\ldots,p_{n+1})|\, \mathcal{O}_{n+1}(p_1,\ldots,p_{n+1}) \\ &+\ \alpha_s^{n-1}(\mu_R^2) \int d\Phi_n\, 2\mathrm{Re}\big(M_n(p_1,\ldots,p_n) \\ &M^*_{n,1-\mathrm{loop}}(p_1,\ldots,p_n)\big)\, \mathcal{O}_n(p_1,\ldots,p_n)\ .\end{aligned} \tag{9.18}$$

Relative to LO calculations, two important issues appear in the NLO calculations. Firstly, the extra complexity of loop-calculations relative to tree-level calculations means that they have yet to be fully automated, though considerable progress is being made in this direction (see Refs. 57–60 and references therein). Secondly, loop amplitudes are infinite in 4 dimensions, while tree-level amplitudes are finite, but their *integrals* are infinite, due to the divergences of Eq. (9.16). These two sources of infinities have the same soft and collinear origins and cancel after the integration only if the observable $\mathcal{O}$ satisfies the property of infrared and collinear safety,

$$\begin{aligned} \mathcal{O}_{n+1}(p_1,\ldots,p_s,\ldots,p_n) &\to \mathcal{O}_n(p_1,\ldots,p_n) \qquad \text{if } p_s \to 0 \\ \mathcal{O}_{n+1}(p_1,\ldots,p_a,p_b,\ldots,p_n) &\to \mathcal{O}_n(p_1,\ldots,p_a+p_b,\ldots,p_n) \\ &\qquad \text{if } p_a \,||\, p_b\,. \end{aligned} \tag{9.19}$$

Examples of infrared safe quantities include event-shape distributions and jet cross sections (with appropriate jet algorithms, see below). Unsafe quantities include the distribution of the momentum of the hardest QCD particle (which is not conserved under collinear splitting), observables that require the complete absence of radiation in some region of phase-space (e.g. rapidity gaps or 100% isolation cuts, which are affected by soft emissions), or the particle multiplicity (affected by both soft and collinear emissions). The non-cancellation of divergences at NLO due to infrared or collinear unsafety compromises the usefulness not only of the NLO calculation, but also that of a LO calculation, since LO is only an acceptable approximation if one can prove that higher order terms are smaller. Infrared and collinear unsafety usually also imply large non-perturbative effects.

As with LO calculations, the phase-space integrals in Eq. (9.18) are usually carried out by Monte Carlo integration, so as to facilitate the study of arbitrary observables. Various methods exist to obtain numerically efficient cancellation among the different infinities. The most widely used in current NLO computer codes is known as dipole subtraction [61]; other methods that have seen numerous applications include FKS [62] and antenna [63] subtraction.

NLO calculations exist for nearly all $2 \to n$ processes with $n \leq 3$ (and for $1 \to 4$ in $e^+e^- \to \gamma/Z \to$hadrons), as reviewed in Ref. 64. Some of the corresponding codes are public, and those that provide access to multiple processes include NLOJet++ [65] for e^+e^-, DIS, and hadron-hadron processes involving just light partons in the final state, MCFM [66] for hadron-hadron processes with vector bosons and/or heavy quarks in the final state, VBFNLO for vector-boson fusion processes [67], and the Phox family [68] for processes with photons in the final state. The current forefront of NLO calculations is $2 \to 4$ processes in pp scattering, for which results exist on $t\bar{t}b\bar{b}$ [59,60] and $pp \to W+3$jets [57,58].

NNLO. Conceptually, NNLO and NLO calculations are similar, except that one must add a further order in α_s, consisting of: the squared $(n+2)$-parton tree-level amplitude, the interference of the $(n+1)$-parton tree-level and 1-loop amplitudes, the interference of the n-parton tree-level and 2-loop amplitudes, and the squared n-parton 1-loop amplitude.

Each of these elements involves large numbers of soft and collinear divergences. Arranging for their cancellation after numerical Monte Carlo integration is one of the

significant challenges of NNLO calculations, as is the determination of the relevant 2-loop amplitudes. The processes for which fully exclusive NNLO calculations exist include the 3-jet cross section in e^+e^- collisions [69,70] (for which NNLO means α_s^3), as well as vector- [71,72] and Higgs-boson [73,74] production in pp and $p\bar{p}$ collisions (for which NNLO means α_s^2).

9.2.2.3. *Resummation:*

Many experimental measurements place tight constraints on emissions in the final state, for example, in e^+e^- events, that the thrust should be less than some value $\tau \ll 1$, or in $pp \to Z$ events that the Z-boson transverse momentum should be much smaller than its mass, $p_{t,Z} \ll M_Z$. A further example is the production of heavy particles or jets near threshold (so that little energy is left over for real emissions) in DIS and pp collisions.

In such cases the constraint vetoes a significant part of the integral over the soft and collinear divergence of Eq. (9.16). As a result, there is only a partial cancellation between real emission terms (subject to the constraint) and loop (virtual) contributions (not subject to the constraint), causing each order of α_s to be accompanied by a large coefficient $\sim L^2$, where *e.g.* $L = \ln\tau$ or $L = \ln(M_Z/p_{t,Z})$. One ends up with a perturbative series whose terms go as $\sim (\alpha_s L^2)^n$. It is not uncommon that $\alpha_s L^2 \gg 1$, so that the perturbative series converges very poorly if at all.** In such cases one may carry out a "resummation," which accounts for the dominant logarithmically enhanced terms to all orders in α_s, by making use of known properties of matrix elements for multiple soft and collinear emissions, and of the all-orders properties of the divergent parts of virtual corrections, following original works such as Refs. 75–84 (or more recently through soft-collinear effective theory, cf. the review in Ref. 85).

For cases with double logarithmic enhancements (two powers of logarithm per power of α_s), there are two classification schemes for resummation accuracy. Writing the cross section including the constraint as $\sigma(L)$ and the unconstrained (total) cross section as $\sigma_{\rm tot}$, the series expansion takes the form

$$\sigma(L) \simeq \sigma_{\rm tot} \sum_{n=0}^{\infty} \sum_{k=0}^{2n} R_{nk} \alpha_s^n(\mu_R^2) L^k, \qquad L \gg 1 \tag{9.20}$$

and leading log (LL) resummation means that one accounts for all terms with $k = 2n$, next-to-leading-log (NLL) includes additionally all terms with $k = 2n-1$, *etc.*. Often

** To be precise one should distinguish two causes of the divergence of perturbative series. That which interests us here is associated with the presence of a new large parameter (*e.g.* ratio of scales). Nearly all perturbative series also suffer from "renormalon" divergences $\alpha_s^n n!$ (reviewed in Ref. 15), which however have an impact only at very high perturbative orders and have a deep connection with non-perturbative uncertainties.

$\sigma(L)$ (or its Fourier or Mellin transform) *exponentiates* [‡],

$$\sigma(L) \simeq \sigma_{\rm tot} \exp\left[\sum_{n=1}^{\infty}\sum_{k=0}^{n+1} G_{nk}\alpha_s^n(\mu_R^2)L^k\right], \qquad L \gg 1\,, \tag{9.21}$$

where one notes the different upper limit on k compared to Eq. (9.20). This is a more powerful form of resummation: the G_{12} term alone reproduces the full LL series in Eq. (9.20). With the form Eq. (9.21) one still uses the nomenclature LL, but this now means that all terms with $k = n + 1$ are included, and NLL implies all terms with $k = n$, *etc.*.

For a large number of observables, the state-of-the art for resummation is NLL in the sense of Eq. (9.21) (see Refs. 89–91 and references therein). NNLL has been achieved for the DY and Higgs-boson p_t distributions [92,93] (in addition the NLL ResBos program [94] is still widely used), the back-to-back energy-energy correlation in e^+e^- [95], and the production of top anti-top pairs near threshold [96–100]. Finally, the parts believed to be dominant in the N^{3}LL resummation are available for the thrust variable in e^+e^- annihilations [101], and for Higgs- and vector-boson production near threshold [102,103] in hadron collisions. The inputs and methods involved in these various calculations are somewhat too diverse to discuss in detail here, so we recommend that the interested reader consults the original references for further details.

9.2.2.4. *Fragmentation functions:*

Since the parton-hadron transition is non-perturbative, it is not possible to perturbatively calculate quantities such as the energy-spectra of specific hadrons in high-energy collisions. However, one can factorize perturbative and non-perturbative contributions via the concept of fragmentation functions. These are the final-state analogue of the parton distribution functions that are used for initial-state hadrons.

It should be added that if one ignores the non-perturbative difficulties and just calculates the energy and angular spectrum of partons in perturbative QCD with some low cutoff scale $\sim \Lambda$ (using resummation to sum large logarithms of $\sqrt{s}/\Lambda$), then this reproduces many features of the corresponding hadron spectra. This is often taken to suggest that hadronization is "local" in momentum space.

Sec. 17 of this *Review* provides further information (and references) on these topics, including also the question of heavy-quark fragmentation.

[‡] Whether or not this happens depends on the quantity being resummed. A classic example involves jet rates in e^+e^- collisions as a function of a jet-resolution parameter $y_{\rm cut}$. The logarithms of $1/y_{\rm cut}$ exponentiate for the k_t (Durham) jet algorithm [86], but not [87] for the JADE algorithm [88] (both are discussed below in Sec. 9.3.1.1).

9.2.2.5. *Parton-shower Monte Carlo generators:*

Parton-shower Monte Carlo (MC) event generators like PYTHIA [104–106], HERWIG [107–109], SHERPA [110], and ARIADNE [111] provide fully exclusive simulations of QCD events. Because they provide access to "hadron-level" events they are a crucial tool for all applications that involve simulating the response of detectors to QCD events. Here we give only a brief outline of how they work and refer the reader to [112] and references therein for a more complete overview.

The MC generation of an event involves several stages. It starts with the random generation of the kinematics and partonic channels of whatever *hard scattering process* the user has requested.

This is then followed by a *parton shower*, usually based on a resummed calculation of the probability $\Delta(Q_0, Q_1)$ for each parton, that it does not split into other partons (e.g. radiate a gluon) between the hard scale Q_0 and some smaller scale Q_1. $\Delta(Q_0, Q_1)$, known as a Sudakov form factor, takes the form $\Delta(Q_0, Q_1) \sim \exp(-G_{12}\alpha_s \ln^2(Q_0/Q_1) + \ldots)$. By choosing a random number r uniformly in the range $0 < r < 1$ and finding the Q_1 value that solves $r = \Delta(Q_0, Q_1)$, the MC determines the scale of the first emission of the shower. The procedure is repeated to obtain Q_2, the scale of the next emission, and so forth down to a scale ~ 1 GeV that separates the perturbative and non-perturbative part of the simulation.

Once it has generated a partonic configuration, the MC "hadronizes" it according to some *hadronization* model. One widely-used model involves stretching a color "string" across quarks and gluons, and breaking it up into hadrons [113,114]. For a discussion of the implementation of this "Lund" model in the MC program PYTHIA, with further improvements and extensions, see Ref. 104 and references therein. Another model breaks each gluon into a $q\bar{q}$ pair and then groups quarks and anti-quarks into colorless "clusters", which then give the hadrons. This cluster hadronization is implemented in the HERWIG event generator [107–109].

For processes with initial-state hadrons, the showering off the incoming partons must additionally take into account the scale-dependence of the PDFs and the non-perturbative part must account also for the proton remnants. In pp and γp scattering, the collision between the hadron remnants generates an *underlying event* (UE), usually by implementing additional $2 \to 2$ scatterings ("multiple parton interactions") at a scale of a few GeV. The separation between the UE and other parts of the shower and hadronization is somewhat ambiguous, because they are all interconnected in terms of their color flow.

Parton showers usually generate a correct distribution of soft and collinear emission, but they often fail to reproduce the pattern of hard wide-angle emissions that would be given by the exact multi-parton matrix elements. In cases where this matters, it is usual to "merge" the parton showers with the generation of exact LO multi-parton matrix elements (Sec. 9.2.2.2), including a prescription to avoid double or under-counting of real and virtual corrections (*e.g.* CKKW [115] or MLM prescriptions [116]) .

MCs as described above generate cross sections for the requested hard process that are correct at LO. For hadron-collider applications it is common to multiply these cross sections by an inclusive K-factor, *i.e.* the ratio of (N)NLO to LO results for a

related inclusive cross section. For measurements with cuts, this may not always be adequate: higher-order corrections in a restricted phase-space region can be substantially different from those in the inclusive case. For a number of processes there also exist MC implementations that are correct to NLO, using the MC@NLO [117] or POWHEG [118] prescriptions to avoid double counting the approximate NLO pieces already implicitly included in the MCs through their showering.

9.2.3. *Accuracy of predictions* :

LO calculations are often said to be accurate to within a factor of two. This is based on the observed impact of scale variation across a range of observables and of the experience with NLO corrections in the cases where these are available. In processes involving new partonic scattering channels at NLO and/or large ratios of scales (such as the production of high-p_t jets containing B-hadrons), the NLO to LO K-factors can be substantially larger than 2.

The accuracy of a given particular perturbative QCD prediction is usually estimated by varying the renormalization and factorization scales around a central value Q that is taken close to the physical scale of the process.[‡‡] A conventional range of variation is $Q/2 < \mu_R, \mu_F < 2Q$.

There does not seem to be a broad consensus on whether μ_R and μ_F should be kept identical or varied independently. One option is to vary them independently with the restriction $\frac{1}{2}\mu_R < \mu_F < 2\mu_R$ [119]. This limits the risk of misleadingly small uncertainties due to fortuitous cancellations between the μ_F and μ_R dependence when both are varied together, while avoiding the appearance of large logarithms of μ_R^2/μ_F^2 when both are varied completely independently.

Calculations that involve resummations usually have an additional source of uncertainty associated with the choice of argument of the logarithms being resummed, *e.g.* $\ln(2\frac{p_{t,Z}}{M_Z})$ as opposed to $\ln(\frac{1}{2}\frac{p_{t,Z}}{M_Z})$. In addition to varying renormalization and factorization scales, it is therefore also advisable to vary the argument of the logarithm by a factor of two in either direction with respect to the "natural" argument.

The accuracy of QCD predictions is limited also by non-perturbative corrections, which typically scale as a power of Λ/Q. For measurements that are directly sensitive to the structure of the hadronic final state the corrections are usually linear in Λ/Q. The non-perturbative corrections are further enhanced in processes with a significant underlying event (*i.e.* in pp and $p\bar{p}$ collisions) and in cases where the perturbative cross sections fall steeply as a function of p_t or some other kinematic variable.

Non-perturbative corrections are commonly estimated from the difference between Monte Carlo events at the parton-level and after hadronization, though methods exist also to analytically deduce non-perturbative effects in one observable based on measurements of other observables (see the reviews [15,120]) .

[‡‡] A more conservative scheme is to take the uncertainty to be the size of the last known perturbative order.

9.3. Experimental QCD

Since we are not able to directly measure partons (quarks or gluons), but only hadrons and their decay products, a central issue for every experimental test of QCD is establishing a correspondence between observables obtained at the partonic and the hadronic level. The only theoretically sound correspondence is achieved by means of *infrared and collinear safe* quantities, which allow one to obtain finite predictions at any order of perturbative QCD.

As stated above, the simplest case of infrared and collinear safe observables are total cross sections. More generally, when measuring inclusive observables, the final state is not analyzed at all regarding its (topological, kinematical) structure or its composition. Basically the relevant information consists in the rate of a process ending up in a partonic or hadronic final state. In e^+e^- annihilation, widely used examples are the ratios of partial widths or branching ratios for the electroweak decay of particles into hadrons or leptons, such as Z or τ decays, (cf. Sec. 9.2.1). Such ratios are often favored over absolute cross sections or partial widths because of large cancellations of experimental and theoretical systematic uncertainties. The strong suppression of non-perturbative effects, $\mathcal{O}(\Lambda^4/Q^4)$, is one of the attractive features of such observables, however, at the same time the sensitivity to radiative QCD corrections is small, which for example affects the statistical uncertainty when using them for the determination of the strong coupling constant. In the case of τ decays not only the hadronic branching ratio is of interest, but also moments of the spectral functions of hadronic tau decays, which sample different parts of the decay spectrum and thus provide additional information. Other examples of inclusive observables are structure functions (and related sum rules) in DIS. These are extensively discussed in Sec. 16 of this *Review*.

As soon as (parts) of the structure or composition of the final state are analyzed and cross section differential in one or more variables characterizing this structure are of interest, we talk about exclusive observables, such as jet rates, jet substructure and event-shape distributions. Furthermore, any cross section differential in some characteristic kinematic quantity of the final state falls into this category, such as transverse momentum distributions of jets or vector bosons in hadron collisions. The case of fragmentation functions, *i.e.* the measurement of hadron production as a function of the hadron momentum relative to some hard scattering scale, is discussed in Sec. 17 of this *Review*.

It is worth mentioning that, besides the correspondence between the parton and hadron level, also a correspondence between the hadron level and the actually measured quantities in the detector has to be established. The simplest examples are corrections for finite experimental acceptance and efficiencies. However, measurements of exclusive observables such as jet rates require more involved corrections in order to relate, *e.g.* the energy deposits in a calorimeter to the jets at the hadron level. Typically detector simulations are used in order to obtain these corrections. Care should be taken here in order to have a clear separation between the parton-to-hadron level and hadron-to-detector level corrections, as well as to ensure the independence of the latter from the MC model used in the simulations. Finally, it is strongly suggested to provide, whenever possible, measurements corrected for detector effects which then can be easily compared to the

results of other experiments and/or theoretical calculations.

9.3.1. *Hadronic final-state observables* :

9.3.1.1. *Jets:*

In hard interactions, final-state partons and hadrons appear predominantly in collimated bunches. These bunches are generically called *jets*. To a first approximation, a jet can be thought of as a hard parton that has undergone soft and collinear showering and then hadronization. Jets are used both for testing our understanding and predictions of high-energy QCD processes, and also for identifying the hard partonic structure of decays of massive particles like top quarks.

In order to map observed hadrons onto a set of jets, one uses a *jet definition*. The mapping involves explicit choices: for example when a gluon is radiated from a quark, for what range of kinematics should the gluon be part of the quark jet, or instead form a separate jet? Good jet definitions are infrared and collinear safe, simple to use in theoretical and experimental contexts, applicable to any type of inputs (parton or hadron momenta, charged particle tracks, and/or energy deposits in the detectors) and lead to jets that are not too sensitive to non-perturbative effects. An extensive treatment of the topic of jet definitions is given in Ref. 121 (for e^+e^- collisions) and Refs. 122, 123 (for pp or $p\bar{p}$ collisions). Here we briefly review the two main classes: cone algorithms, extensively used at hadron colliders, and sequential recombination algorithms, more widespread in e^+e^- and ep colliders.

Very generically, most (iterative) cone algorithms start with some seed particle i, sum the momenta of all particles j within a cone of opening-angle R, typically defined in terms of (pseudo-)rapidity and azimuthal angle. They then take the direction of this sum as a new seed and repeat until the cone is stable, and call the contents of the resulting stable cone a jet if its transverse momentum is above some threshold $p_{t,\mathrm{min}}$. The parameters R and $p_{t,\mathrm{min}}$ should be chosen according to the needs of a given analysis.

There are many variants of cone algorithm, and they differ in the set of seeds they use and the manner in which they ensure a one-to-one mapping of particles to jets, given that two stable cones may share particles ("overlap"). The use of seed particles is a problem w.r.t. infrared and collinear safety, and seeded algorithms are generally not compatible with higher-order (or sometimes even leading-order) QCD calculations, especially in multi-jet contexts, as well as potentially subject to large non-perturbative corrections and instabilities. Seeded algorithms (JetCLU, MidPoint, and various other experiment-specific iterative cone algorithms) are therefore to be deprecated. A modern alternative is to use a seedless variant, SISCone [124].

Sequential recombination algorithms at hadron colliders (and in DIS) are characterized by a distance $d_{ij} = \min(k_{t,i}^{2p}, k_{t,j}^{2p})\Delta_{ij}^2/R^2$ between all pairs of particles i, j, where Δ_{ij} is their distance in the rapidity-azimuthal plane, $k_{t,i}$ is the transverse momentum w.r.t. the incoming beams, and R is a free parameter. They also involve a "beam" distance $d_{iB} = k_{t,i}^{2p}$. One identifies the smallest of all the d_{ij} and d_{iB}, and if it is a d_{ij}, then i and j are merged into a new pseudo-particle (with some prescription, a recombination scheme, for the definition of the merged four-momentum). If the smallest distance is a d_{iB}, then i

is removed from the list of particles and called a jet. As with cone algorithms, one usually considers only jets above some transverse-momentum threshold $p_{t,\min}$. The parameter p determines the kind of algorithm: $p = 1$ corresponds to the (*inclusive-*)k_t algorithm [86,125,126], $p = 0$ defines the *Cambridge-Aachen* algorithm [127,128], while for $p = -1$ we have the *anti-*k_t algorithm [129]. All these variants are infrared and collinear safe to all orders of perturbation theory. Whereas the former two lead to irregularly shaped jet boundaries, the latter results in cone-like boundaries.

The k_t algorithm in e^+e^- annihilations [86] uses $y_{ij} = 2\,\min(E_i^2, E_j^2)(1-\cos\theta_{ij})/Q^2$ as distance measure and repeatedly merges the pair with smallest y_{ij}, until all y_{ij} distances are above some threshold $y_{\rm cut}$, the jet resolution parameter. The (pseudo)-particles that remain at this point are called the jets. Here it is $y_{\rm cut}$ (rather than R and $p_{t,\min}$) that should be chosen according to the needs of the analysis. As mentioned above, the k_t algorithm has the property that logarithms $\ln(1/y_{\rm cut})$ exponentiate in resummation calculations. This is one reason why it is preferred over the earlier JADE algorithm [88], which uses the distance measure $y_{ij} = 2\,E_i\,E_j\,(1-\cos\theta_{ij})/Q^2$.

Efficient implementations of the above algorithms are available through the *FastJet* package [130], which is also packaged within *SpartyJet* [131].

9.3.1.2. *Event Shapes:*

Event-shape variables are functions of the four momenta in the hadronic final state that characterize the topology of an event's energy flow. They are sensitive to QCD radiation (and correspondingly to the strong coupling) insofar as gluon emission changes the shape of the energy flow.

The classic example of an event shape is the *thrust* [132,133] in e^+e^- annihilations, defined as

$$\hat{\tau} = \max_{\vec{n}_\tau} \frac{\sum_i |\vec{p}_i \cdot \vec{n}_\tau|}{\sum_i |\vec{p}_i|}\,, \tag{9.22}$$

where $\vec{p}_i$ are the momenta of the final-state particles and the maximum is obtained for the thrust axis $\vec{n}_\tau$. In the Born limit of the production of a perfect back-to-back $q\bar{q}$ pair the limit $\hat{\tau} \to 1$ is obtained, whereas a perfectly symmetric many-particle configuration leads to $\hat{\tau} \to 1/2$. Further event shapes of similar nature have been defined and extensively measured at LEP and at HERA, and for their definitions and reviews we refer to Refs. 1,2,120,134,135. Some discussion of hadron-collider event shapes is given in Ref. 136.

Event shapes are used for many purposes. These include measuring the strong coupling, tuning the parameters of Monte Carlo showering programs, investigating analytical models of hadronization and distinguishing QCD events from events that might involve decays of new particles (giving event-shape values closer to the spherical limit).

9.3.1.3. *Jet substructure, quark vs. gluon jets:*

Jet substructure, which can be resolved by finding subjets or by measuring jet shapes, is sensitive to the details of QCD radiation in the shower development inside a jet and has been extensively used to study differences in the properties of quark and gluon induced jets, strongly related to their different color charges. In general there is clear experimental evidence that gluon jets are "broader" and have a softer particle spectrum than (light-) quark jets, whereas b-quark jets are similar to gluon jets. As an example for an observable, the jet shape $\Psi(r/R)$ is the fractional transverse momentum contained within a sub-cone of cone-size r for jets of cone-size R. It is sensitive to the relative fractions of quark and gluon jets in an inclusive jet sample and receives contributions from soft-gluon initial-state radiation and beam remnant-remnant interactions. Therefore, it has been widely employed for validation and tuning of Monte Carlo models. CDF has measured the jet shape $\Psi(r/R)$ for an inclusive jet sample [137] as well as for b-jets [138]. Similar measurements in DIS have been reported in Refs. 139, 140. Further discussions, references and, recent summaries can be found in Refs. 135, 141, 142.

The use of jet substructure has also been suggested in order to distinguish QCD jets from jets that originate from hadronic decays of boosted massive particles (high-p_t electroweak bosons, top quarks and hypothesized new particles). For a review and detailed references, see sec. 5.3 of Ref. 122.

9.3.2. ***State of the art QCD measurements at colliders*** :

There exists an enormous wealth of data on QCD-related measurements in e^+e^-, ep, pp, and $p\bar{p}$ collisions, to which a short overview like this would not be able to do any justice. Extensive reviews of the subject have been published in Refs. 134, 135 for e^+e^- colliders, whereas for hadron colliders comprehensive overviews are given in Refs. 123, 143, and recent summaries can be found in, *e.g.* Refs. 144–146, 142. Below we concentrate our discussion on measurements that are most sensitive to hard QCD processes.

9.3.2.1. e^+e^- *colliders:* The analyses of jet production in e^+e^- collisions, mostly from JADE data at center-of-mass energies between 14 and 44 GeV, as well as from LEP data at the Z resonance and up to 209 GeV, covered the measurements of (differential or exclusive) jet rates (with multiplicities typically up to 4, 5 or 6 jets), the study of 3-jet events and particle production between the jets as a tool for testing hadronization models, as well as 4-jet production and angular correlations in 4-jet events, useful for measurements of the strong coupling constant and putting constraints on the QCD color factors, thus probing the non-abelian nature of QCD. There have also been extensive measurements of event shapes. The tuning of parton shower MC models, typically matched to matrix elements for 3-jet production, has led to good descriptions of the available, highly precise data. Especially for the large LEP data sample at the Z peak, the statistical errors are mostly negligible, whereas the experimental systematic uncertainties are at the per-cent level or even below. These are usually dominated by the uncertainties related to the MC model dependence of the efficiency and acceptance corrections (often referred to as "detector corrections").

9.3.2.2. *DIS and photoproduction:* Multi-jet production in ep collisions at HERA, both in the DIS and photoproduction regime, allows for tests of QCD factorization (one initial-state proton and its associated PDF versus the hard scattering which leads to high-p_t jets) and NLO calculations which exist for 2- and 3-jet final states. Sensitivity is also obtained to the product of the coupling constant and the gluon PDF. By now experimental uncertainties of the order of $5-10\%$ have been achieved, mostly dominated by jet energy scale uncertainties, whereas statistical errors are negligible to a large extent. For comparison to theoretical predictions, at large jet p_t the PDF uncertainty dominates the theoretical error (typically of order 5 - 10%, in some regions of phase-space up to 20%), therefore jet observables become useful inputs for PDF fits. In general, for Q^2 above $\sim 100\,\mathrm{GeV}^2$ the data are well described by NLO matrix element calculations, combined with DGLAP evolution equations. Results at lower values ($Q^2 < 100\,\mathrm{GeV}^2$) point to the necessity of including NNLO effects. Also, at low values of Q^2 and x, in particular for large jet pseudo-rapidities, there are indications for the need of BFKL-type evolution, though the predictions for such schemes are still limited. In the case of photoproduction, the data-theory comparisons are hampered by the uncertainties related to the photon PDF.

A few examples of recent measurements can be found in Refs. 147–150 for DIS and in Refs. 151–153 for photoproduction.

9.3.2.3. *Hadron colliders:* Jet measurements at the TEVATRON are now published for data samples up to $\sim 2\,\mathrm{fb}^{-1}$. Among the most important cross sections measured is the inclusive jet production as a function of the jet transverse energy (E_t) or the jet transverse momentum (p_t), now available for several rapidity regions and for p_t up to 700 GeV. Most notably, the TEVATRON experiments now have measurements based on the infrared- and collinear-safe k_t algorithm in addition to the more widely used Midpoint and JetCLU algorithms of the past. Recent results by the CDF and D0 collaborations can be found in Refs. 154, 155, where we observe a good description of the data by the NLO QCD predictions. The experimental systematic uncertainties are dominated by the jet energy scale error, by now quoted to less than 3% and thus leading to uncertainties of 10 to 60% on the cross section, increasing with p_t. The PDF uncertainties dominate the theoretical error. In fact, inclusive jet data are important inputs to global PDF fits, in particular for constraining the high-x gluon PDF.

A rather comprehensive summary, comparing NLO QCD predictions to data for inclusive jet production in DIS, pp, and $p\bar{p}$ collisions, is given in Ref. 156 and reproduced here in Fig. 9.1.

Dijet events are analyzed in terms of their invariant mass and angular distributions, which allow one to put stringent limits on deviations from the Standard Model, such as quark compositeness (two recent examples can be found in Refs. 158, 159). Furthermore, dijet azimuthal correlations between the two leading jets, normalized to the total dijet cross cross section, are an extremely valuable tool for studying the spectrum of gluon radiation in the event. As shown in Ref. 160, the LO (non-trivial) prediction for this observable, with at most three partons in the final state, is not able to describe the data for an azimuthal separation below $2\pi/3$, where NLO contributions (with 4 partons)

restore the agreement with data. In addition, this observable can be employed to tune Monte Carlo predictions of soft gluon radiation in the final state.

Similarly important tests of QCD arise from measurements of vector boson (photon, W, Z) production together with jets. A recent analysis of photon+jet production by D0 [161] indicates that NLO calculations, combined with modern PDF sets, are unable to describe the shape of the photon p_t across the entire measured range, showing the need for an improved and consistent theoretical description of this process.

In the case of Z+jets, the Z momentum can be precisely reconstructed using the leptons, allowing for a precise determination of the Z p_t distribution, which is sensitive to QCD radiation both at high and low scales and thus probes perturbative as well as non-perturbative effects. For example, a recent D0 result [162] quotes experimental statistical and systematic uncertainties of the order of 10%, increasing up to 20% in the lowest momentum range. The data are compared to predictions from NLO QCD and from different Monte Carlo models, where, for example, LO matrix elements for up to three partons are matched to a parton shower. Whereas the total cross section is underestimated, the shape is well reproduced over a large phase-space region. Further examples of recent results for Z (or W) plus jets production are found in Refs. 161, 163, 164. Among the most important recent developments is the completion of a NLO calculation for W+3jet production [57,58], which will be relevant also for future LHC background estimations. This type of process is an example, where jets need to be found with an infrared and collinear safe jet algorithm, such as SISCone, in order to obtain finite NLO predictions. This would not be possible with algorithms such as Midpoint or JetCLU. The latter is used for a CDF measurement [164], which is compared to the NLO QCD prediction with SISCone as jet algorithm. Besides this inconsistency, the agreement appears to be good.

Finally, TEVATRON measurements of heavy quark (b, c) jet production, inclusive or in association with vector bosons, have led to stringent tests of NLO predictions (see Refs. 165–170 for examples of recent analyses).

9.3.3. *Tests of the non-abelian nature of QCD* :

QCD is a gauge theory with SU(3) as underlying gauge group. For a general gauge theory with a simple Lie group, the couplings of the fermion fields to the gauge fields and the self-interactions in the non-abelian case are determined by the coupling constant and Casimir operators of the gauge group, as introduced in Sec. 9.1. Measuring the eigenvalues of these operators, called color factors, probes the underlying structure of the theory in a gauge invariant way and provides evidence of the gluon self-interactions. Typically, cross sections can be expressed as functions of the color factors, for example $\sigma = f(\alpha_s C_F, C_A/C_F, n_f T_R/C_F)$. Sensitivity at leading order in perturbation theory can be achieved by measuring angular correlations in 4-jet events in e^+e^- annihilation or 3-jet events in DIS. Some sensitivity, although only at NLO, is also obtained from event-shape distributions. Scaling violations of fragmentation functions and the different subjet structure in quark and gluon induced jets also give access to these color factors. In order to extract absolute values, *e.g.* for C_F and C_A, certain assumptions have to be made for other parameters, such as T_R, n_f or α_s, since

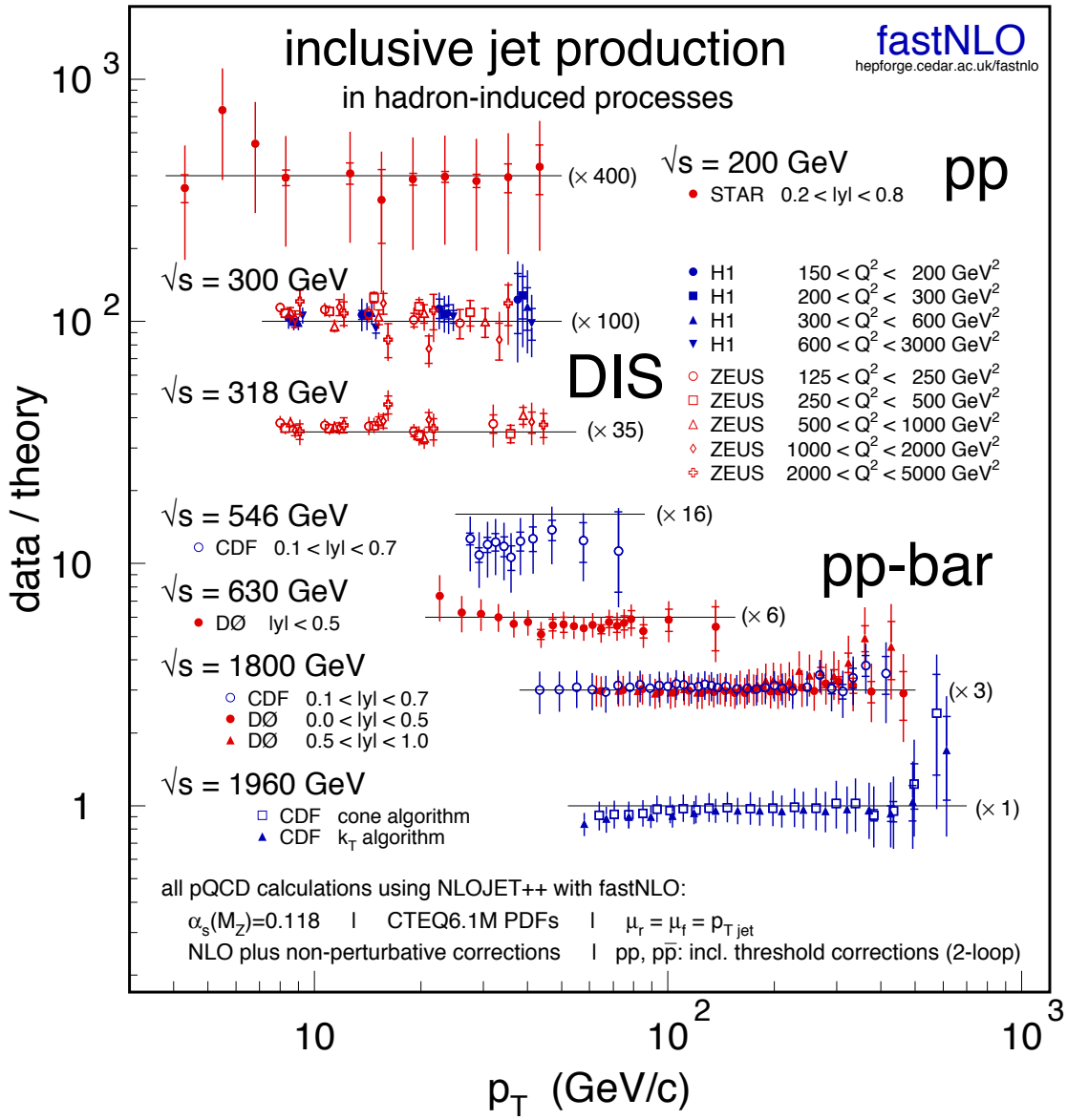

Figure 9.1: A compilation of data-over-theory ratios for inclusive jet cross sections as a function of jet transverse momentum (p_T), measured in different hadron-induced processes at different center-of-mass energies; from Ref. 156, including some updates [157]. The various ratios are scaled by arbitrary numbers (indicated between parentheses) for better readability of the plot. The theoretical predictions have been obtained at NLO accuracy, for parameter choices (coupling constant, PDFs, renormalization, and factorization scales) as indicated at the bottom of the figure. Color version at end of book.

typically only combinations (ratios, products) of all the relevant parameters appear in the perturbative prediction. A recent compilation of results [135] quotes world average values of $C_A = 2.89 \pm 0.03(\text{stat}) \pm 0.21(\text{syst})$ and $C_F = 1.30 \pm 0.01(\text{stat}) \pm 0.09(\text{syst})$, with a correlation coefficient of 82%. These results are in perfect agreement with the

expectations from SU(3) of $C_A = 3$ and $C_F = 4/3$. An overview of the history and the current status of tests of asymptotic freedom, closely related to the non-abelian nature of QCD, can be found in Ref. 171.

9.3.4. *Measurements of the strong coupling constant* :

If the quark masses are fixed, there is only one free parameter in the QCD Lagrangian, the strong coupling constant α_s. The coupling constant in itself is not a physical observable, but rather a quantity defined in the context of perturbation theory, which enters predictions for experimentally measurable observables, such as R in Eq. (9.7).

Many experimental observables are used to determine α_s. Considerations in such determinations include:

- The observable's sensitivity to α_s as compared to the experimental precision. For example, for the e^+e^- cross section to hadrons (cf. R in Sec. 9.2.1), QCD effects are only a small correction, since the perturbative series starts at order α_s^0; 3-jet production or event shapes in e^+e^- annihilations are directly sensitive to α_s since they start at order α_s; the hadronic decay width of heavy quarkonia, $\Gamma(\Upsilon \to \text{hadrons})$, is very sensitive to α_s since its leading order term is $\propto \alpha_s^3$.
- The accuracy of the perturbative prediction, or equivalently of the relation between α_s and the value of the observable. The minimal requirement is generally considered to be an NLO prediction. Some observables are predicted to NNLO (many inclusive observables, 3-jet rates and event shapes in e^+e^- collisions) or even N^{3}LO (e^+e^- hadronic cross section and τ branching fraction to hadrons). In certain cases, fixed-order predictions are supplemented with resummation. The precise magnitude of theory uncertainties is usually estimated as discussed in Sec. 9.2.3.
- The size of uncontrolled non-perturbative effects (except for lattice-based determinations of α_s). Sufficiently inclusive quantities, like the e^+e^- cross section to hadrons, have small non-perturbative uncertainties $\sim \Lambda^4/Q^4$. Others, such as event-shape distributions, have uncertainties $\sim \Lambda/Q$.
- The scale at which the measurement is performed. An uncertainty δ on a measurement of $\alpha_s(Q^2)$, at a scale Q, translates to an uncertainty $\delta' = (\alpha_s^2(M_Z^2)/\alpha_s^2(Q^2)) \cdot \delta$ on $\alpha_s(M_Z^2)$. For example, this enhances the already important impact of precise low-Q measurements, such as from τ decays, in combinations performed at the M_Z scale.

In this review, we make no attempt to compile a full list of measurements of α_s or to produce a new world average value from them. We rather prefer to quote a recent analysis by Bethke [172], which incorporates results with recently improved theoretical predictions and/or experimental precision[♯]. For detailed comments on the selected set of recent results we refer to Ref. 172. Here we quote the main inputs:

- Several re-analyses of the hadronic τ decay width [16,174–179], based on the new N^{3}LO predictions, have been performed, with different approaches towards the detailed treatment of the perturbative (fixed order or contour improved

[♯] The time evolution of α_s combinations can be followed by consulting Refs. 171, 173 as well as earlier editions of this *Review*.

perturbative expansions) and non-perturbative contributions. In Ref. 172 a value of $\alpha_s(M_Z^2) = 0.1197 \pm 0.0016$ is quoted as average, where the uncertainty spans the difference of those recent analyses.

- The N^{3}LO calculation of the hadronic Z decay width was used in a recent revision of the global fit to electroweak precision data [180], resulting in $\alpha_s(M_Z^2) = 0.1193^{+0.0028}_{-0.0027} \pm 0.0005$, where the first error is of experimental and the second of theoretical origin.
- A combined analysis of non-singlet structure functions from DIS [181], based on QCD predictions up to N^{3}LO, gives $\alpha_s(M_Z^2) = 0.1142 \pm 0.0023$. This uncertainty includes a theoretical error of ± 0.0008.
- A recent re-analysis of event shapes, measured by ALEPH at the Z peak and LEP2 energies up to 209 GeV, using NNLO predictions matched to NLL resummation, has resulted in $\alpha_s(M_Z^2) = 0.1224 \pm 0.0039$ [182], with a dominant theoretical uncertainty of 0.0035. Similarly, an analysis of JADE data [183] at center-of-mass energies between 14 and 46 GeV gives $\alpha_s(M_Z^2) = 0.1172 \pm 0.0051$, with contributions from hadronization model (perturbative QCD) uncertainties of 0.0035 (0.0030).
- A new combination [184] of precision measurements at HERA, based on NLO fits to inclusive jet cross sections in neutral current DIS at high Q^2, quotes a combined result of $\alpha_s(M_Z^2) = 0.1198 \pm 0.0032$, which includes a theoretical uncertainty of ± 0.0026.
- An improved extraction of the strong coupling constant from a NLO analysis of radiative Υ decays [185] resulted in $\alpha_s(M_Z) = 0.119^{+0.006}_{-0.005}$.
- The HPQCD collaboration [186] computes Wilson loops and similar short-distance quantities with lattice QCD and analyzes them with NNLO perturbative QCD. This yields a value for α_s, but the lattice scale must be related to a physical energy/momentum scale. This is achieved with the Υ'-Υ mass difference, however, many other quantities could be used as well [187]. HPQCD obtains $\alpha_s(M_Z^2) = 0.1183 \pm 0.0008$, where the uncertainty includes effects from truncating perturbation theory, finite lattice spacing and extrapolation of lattice data. An independent perturbative analysis of the same lattice-QCD data yields $\alpha_s(M_Z^2) = 0.1192 \pm 0.0011$ [188]. The HPQCD value [186] is taken for the average. It is the most precise of all inputs used in Ref. 172. It is worth noting that there is a more recent result in Ref. 189, which avoids the staggered fermion treatment of Ref. 186. There a value of $\alpha_s(M_Z^2) = 0.1205 \pm 0.0008 \pm 0.0005\,^{+0.0000}_{-0.0017}$ [189] is found, where the first uncertainty is statistical and the others are from systematics. Since this approach uses a different discretization of lattice fermions and a different general methodology, it provides an important cross check of other lattice extractions of α_s.

A non-trivial exercise consists in the evaluation of a world-average value for $\alpha_s(M_Z^2)$. A certain arbitrariness and subjective component is inevitable because of the choice of measurements to be included in the average, the treatment of (non-Gaussian) systematic uncertainties of mostly theoretical nature, as well as the treatment of correlations among the various inputs, again mostly of theoretical origin. In Ref. 172 an attempt has been made to take account of such correlations, using methods as proposed, *e.g.*, in Ref. 190.

The central value is determined as the weighted average of the individual measurements. For the error an overall, a-priori unknown, correlation coefficient is introduced and determined by requiring that the total χ^2 of the combination equals the number of degrees of freedom. The world average quoted in Ref. 172 is

$$\alpha_s(M_Z^2) = 0.1184 \pm 0.0007 \ ,$$

with an astonishing precision of 0.6%. It is worth noting that a cross check performed in Ref. 172, consisting in excluding each of the single measurements from the combination, resulted in variations of the central value well below the quoted uncertainty, and in a maximal increase of the combined error up to 0.0012. Most notably, excluding the most precise determination from lattice QCD gives only a marginally different average value. Nevertheless, there remains an apparent and long-standing systematic difference between the results from structure functions and other determinations of similar accuracy. This is evidenced in Fig. 9.2 (left), where the various inputs to this combination, evolved to the Z mass scale, are shown. Fig. 9.2 (right) provides strongest evidence for the correct prediction by QCD of the scale dependence of the strong coupling.

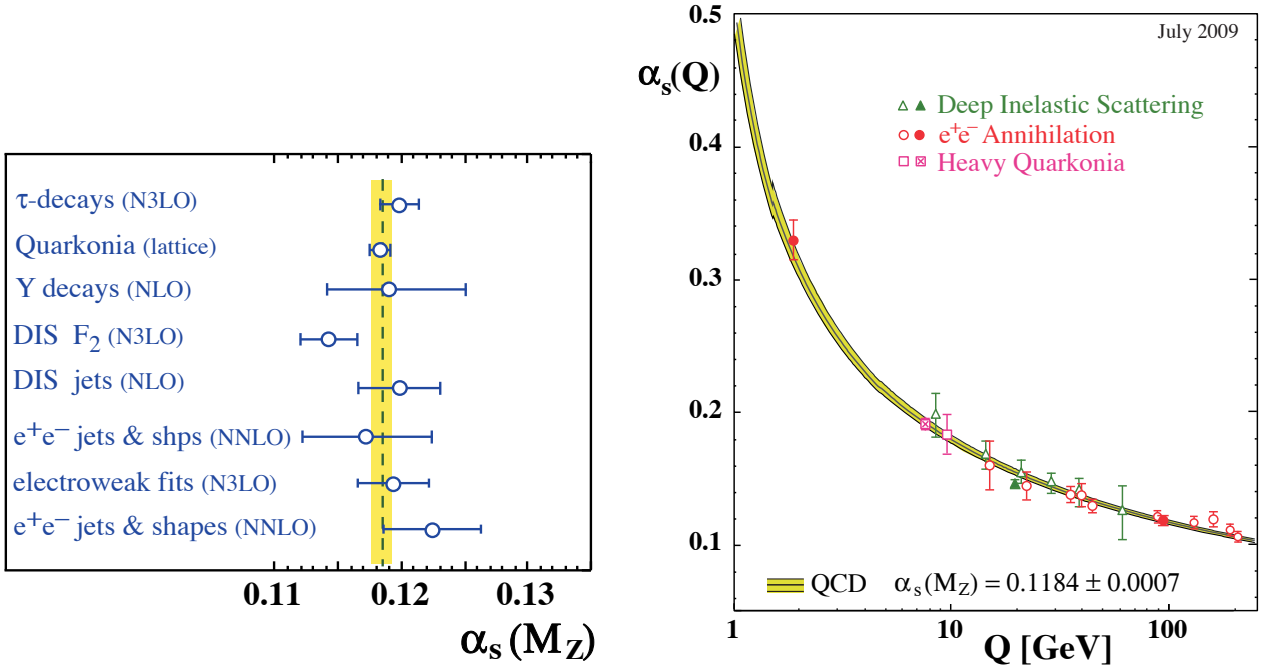

Figure 9.2: Left: Summary of measurements of $\alpha_s(M_Z^2)$, used as input for the world average value; Right: Summary of measurements of α_s as a function of the respective energy scale Q. Both plots are taken from Ref. 172.

9.4. Acknowledgments

We are grateful to S. Bethke, J. Butterworth, M. Cacciari, L. del Debbio, P. Gambino, A. Kronfeld, M. d'Onofrio, S. Sharpe, D. Treille, N. Varelas, M. Wobisch, W.M. Yao, C.P. Yuan, and G. Zanderighi for their suggestions and comments.

References:

1. R.K. Ellis, W.J. Stirling, and B.R. Webber, *"QCD and collider physics," Camb. Monogr. Part. Phys. Nucl. Phys. Cosmol.* **81** (1996).
2. G. Dissertori, I.G. Knowles, and M. Schmelling, *"High energy experiments and theory,"" Oxford, UK: Clarendon* (2003).
3. R. Brock *et al.*, [CTEQ Collaboration], Rev. Mod. Phys. **67**, 157 (1995), see also `http://www.phys.psu.edu/~cteq/handbook/v1.1/handbook.pdf`.
4. J. Smit, *"Introduction to quantum fields on a lattice: A robust mate," Cambridge Lect. Notes Phys.* **15** (2002), p. 1.
5. T. DeGrand and C.E. Detar, *Lattice methods for quantum chromodynamics,World Scientific* (2006).
6. *"Perspectives in Lattice QCD," Proceedings of the Workshop, Nara International Seminar House (2005)*, Ed. Y. Kuramashi, World Scientific 2008.
7. T. Onogi, `arXiv:0906.2344 [hep-ph]`.
8. D. d'Enterria, `arXiv:0902.2488 [nucl-ex]`.
9. T. van Ritbergen, J.A.M. Vermaseren, and S.A. Larin, Phys. Lett. **B400**, 379 (1997) `[arXiv:hep-ph/9701390]`.
10. M. Czakon, Nucl. Phys. **B710**, 485 (2005) `[arXiv:hep-ph/0411261]`.
11. Y. Schroder and M. Steinhauser, JHEP **0601**, 051 (2006) `[arXiv:hep-ph/0512058]`.
12. K.G. Chetyrkin, J.H. Kuhn, and C. Sturm, Nucl. Phys. **B744**, 121 (2006) `[arXiv:hep-ph/0512060]`.
13. K.G. Chetyrkin, B.A. Kniehl, and M. Steinhauser, Nucl. Phys. **B510**, 61 (1998) `[arXiv:hep-ph/9708255]`.
14. See for example section 11.4 of M.E. Peskin and D.V. Schroeder, *"An Introduction To Quantum Field Theory," Reading, USA: Addison-Wesley* (1995), 842 p.
15. M. Beneke, Phys. Reports **317**, 1 (1999) `[arXiv:hep-ph/9807443]`.
16. P.A. Baikov, K.G. Chetyrkin, and J.H. Kuhn, Phys. Rev. Lett. **101**, 012002 (2008) `[arXiv:0801.1821 [hep-ph]]`.
17. P.A. Baikov, K.G. Chetyrkin, and J.H. Kuhn, `arXiv:0906.2987 [hep-ph]`.
18. K.G. Chetyrkin, J.H. Kuhn, and A. Kwiatkowski, Phys. Reports **277**, 189 (1996).
19. M. Spira, Fortsch. Phys. **46**, 203 (1998) `[arXiv:hep-ph/9705337]`.
20. A. Djouadi, Phys. Reports **457**, 1 (2008) `[arXiv:hep-ph/0503172]`.
21. A.H. Hoang, PoS **TOP2006** 032, (2006) `[arXiv:hep-ph/0604185]`.
22. J.M. Zanotti, PoS **LC2008** 051 (2008).
23. V.N. Gribov and L.N. Lipatov, Sov. J. Nucl. Phys. **15**, 438 (1972);
    G. Altarelli and G. Parisi, Nucl. Phys. **B126**, 298 (1977);
    Yu.L. Dokshitzer, Sov. Phys. JETP **46**, 641 (1977).

24. A. Vogt, S. Moch, and J.A.M. Vermaseren, Nucl. Phys. **B691**, 129 (2004) [arXiv:hep-ph/0404111].
25. S. Moch, J.A.M. Vermaseren, and A. Vogt, Nucl. Phys. **B688**, 101 (2004) [arXiv:hep-ph/0403192].
26. J.A.M. Vermaseren, A. Vogt, and S. Moch, Nucl. Phys. **B724**, 3 (2005) [arXiv:hep-ph/0504242].
27. E.B. Zijlstra and W.L. van Neerven, Phys. Lett. **B297**, 377 (1992).
28. S. Moch, J.A.M. Vermaseren, and A. Vogt, arXiv:0812.4168 [hep-ph].
29. E. Laenen *et al.*, Nucl. Phys. **B392**, 162 (1993);
    S. Riemersma, J. Smith, and W.L. van Neerven, Phys. Lett. **B347**, 143 (1995) [arXiv:hep-ph/9411431].
30. I. Bierenbaum, J. Blumlein, and S. Klein, Nucl. Phys. **B820**, 417 (2009) [arXiv:0904.3563 [hep-ph]].
31. J.C. Collins, D.E. Soper, and G. Sterman, Nucl. Phys. **B261**, 104 (1985).
32. R. Hamberg, W.L. van Neerven, and T. Matsuura, Nucl. Phys. **B359**, 343 (1991); Erratum *ibid.*, B **644** 403, (2002).
33. R.V. Harlander and W.B. Kilgore, Phys. Rev. Lett. **88**, 201801 (2002) [arXiv:hep-ph/0201206].
34. C. Anastasiou and K. Melnikov, Nucl. Phys. **B646**, 220 (2002) [arXiv:hep-ph/0207004].
35. V. Ravindran, J. Smith, and W.L. van Neerven, Nucl. Phys. **B665**, 325 (2003) [arXiv:hep-ph/0302135].
36. R.V. Harlander and K. J. Ozeren, arXiv:0909.3420 [hep-ph].
37. M. Greco and A. Vicini, Nucl. Phys. **B415**, 386 (1994).
38. L.N. Lipatov, Sov. J. Nucl. Phys. **23**, 338 (1976) [Yad. Fiz. **23**, 642 (1976)].
39. E.A. Kuraev, L.N. Lipatov, and V.S. Fadin, Sov. Phys. JETP **45**, 199 (1977) [Zh. Eksp. Teor. Fiz. **72**, 377 (1977)].
40. I.I. Balitsky and L.N. Lipatov, Sov. J. Nucl. Phys. **28**, 822 (1978) [Yad. Fiz. **28**, 1597 (1978)].
41. V.S. Fadin and L.N. Lipatov, Phys. Lett. **B429**, 127 (1998) [arXiv:hep-ph/9802290].
42. M. Ciafaloni and G. Camici, Phys. Lett. **B430**, 329 (1998) [arXiv:hep-ph/9803389].
43. S. Marzani *et al.*, Nucl. Phys. **B783**, 143 (2007) [arXiv:0704.2404 [hep-ph]].
44. M. Ciafaloni *et al.*, JHEP **0708**, 046 (2007) [arXiv:0707.1453 [hep-ph]].
45. C.D. White and R.S. Thorne, Phys. Rev. **D75**, 034005 (2007) [arXiv:hep-ph/0611204].
46. I. Balitsky, Nucl. Phys. **B463**, 99 (1996) [arXiv:hep-ph/9509348].
47. Y.V. Kovchegov, Phys. Rev. **D60**, 034008 (1999) [arXiv:hep-ph/9901281].
48. A. Hebecker, Phys. Reports **331**, 1 (2000) [arXiv:hep-ph/9905226].
49. A.V. Belitsky and A.V. Radyushkin, Phys. Reports **418**, 1 (2005) [arXiv:hep-ph/0504030].

50. E. Boos *et al.*, [CompHEP Collaboration], Nucl. Instrum. Methods **A534**, 250 (2004) [arXiv:hep-ph/0403113]; http://comphep.sinp.msu.ru/.
51. J. Alwall *et al.*, JHEP **0709**, 028 (2007) [arXiv:0706.2334 [hep-ph]]; http://madgraph.hep.uiuc.edu/.
52. M.L. Mangano *et al.*, JHEP **0307**, 001 (2003) [arXiv:hep-ph/0206293]; http://cern.ch/mlm/alpgen/.
53. T. Gleisberg and S. Hoche, JHEP **0812**, 039 (2008) [arXiv:0808.3674 [hep-ph]].
54. A. Cafarella, C.G. Papadopoulos, and M. Worek,arXiv: 0710.2427 [hep-ph];http://cern.ch/helac-phegas/.
55. F.A. Berends and W.T. Giele, Nucl. Phys. **B306**, 759 (1988).
56. L.J. Dixon, arXiv:hep-ph/9601359.
57. C.F. Berger *et al.*, arXiv:0907.1984 [hep-ph].
58. R. Keith Ellis, K. Melnikov, and G. Zanderighi, arXiv:0906.1445 [hep-ph].
59. G. Bevilacqua *et al.*, arXiv:0907.4723 [hep-ph].
60. A. Bredenstein *et al.*, arXiv:0905.0110 [hep-ph]].
61. S. Catani and M.H. Seymour, Nucl. Phys. **B485**, 291 (1997) [Erratum-ibid. B **510** (1998) 503] [arXiv:hep-ph/9605323].
62. S. Frixione, Z. Kunszt, and A. Signer, Nucl. Phys. **B467**, 399 (1996) [arXiv:hep-ph/9512328].
63. D.A. Kosower, Phys. Rev. **D57**, 5410 (1998) [arXiv:hep-ph/9710213]; J.M. Campbell, M.A. Cullen, and E.W.N. Glover, Eur. Phys. J. **C9**, 245 (1999) [arXiv:hep-ph/9809429]; D.A. Kosower, Phys. Rev. **D71**, 045016 (2005) [arXiv:hep-ph/0311272].
64. Z. Bern *et al.*, [NLO Multileg Working Group], arXiv:0803.0494 [hep-ph].
65. Z. Nagy, Phys. Rev. **D68**, 094002 (2003) [arXiv:hep-ph/0307268]; http://cern.ch/nagyz/Site/NLOJet++.html.
66. J.M. Campbell and R.K. Ellis, Phys. Rev. **D62**, 114012 (2000) [arXiv:hep-ph/0006304]; http://mcfm.fnal.gov/.
67. K. Arnold *et al.*, Comput. Phys. Commun. **180** 1661, (2009) [arXiv:0811.4559 [hep-ph]]; http://www-itp.particle.uni-karlsruhe.de/∼vbfnloweb/.
68. T. Binoth *et al.*, Eur. Phys. J. **C16**, 311 (2000) [arXiv:hep-ph/9911340]; http://lappweb.in2p3.fr/lapth/PHOX_FAMILY/.
69. A. Gehrmann-De Ridder *et al.*, JHEP **0712**, 094 (2007) [arXiv:0711.4711 [hep-ph]].
70. S. Weinzierl, Phys. Rev. Lett. **101**, 162001 (2008) [arXiv:0807.3241 [hep-ph]]; JHEP **0906**, 041 (2009) [arXiv:0904.1077 [hep-ph]].
71. K. Melnikov and F. Petriello, Phys. Rev. **D74**, 114017 (2006) [arXiv:hep-ph/0609070].
72. S. Catani *et al.*, arXiv:0903.2120 [hep-ph].

73. C. Anastasiou, K. Melnikov, and F. Petriello, Nucl. Phys. **B724**, 197 (2005) [arXiv:hep-ph/0501130].
74. S. Catani and M. Grazzini, Phys. Rev. Lett. **98**, 222002 (2007) [arXiv:hep-ph/0703012].
75. Y.L. Dokshitzer, D.Diakonov, and S.I. Troian, Phys. Reports **58**, 269 (1980).
76. G. Parisi and R. Petronzio, Nucl. Phys. **B154**, 427 (1979).
77. G. Curci, M. Greco, and Y. Srivastava, Nucl. Phys. **B159**, 451 (1979).
78. A. Bassetto, M. Ciafaloni, and G. Marchesini, Nucl. Phys. **B163**, 477 (1980).
79. J.C. Collins and D.E. Soper, Nucl. Phys. **B193**, 381 (1981) [Erratum-*ibid.* **B213**, 545 (1983)].
80. J.C. Collins and D.E. Soper, Nucl. Phys. **B197**, 446 (1982).
81. J. Kodaira and L. Trentadue, Phys. Lett. **B112**, 66 (1982).
82. J. Kodaira and L. Trentadue, Phys. Lett. **B123**, 335 (1983).
83. J.C. Collins, D.E. Soper, and G. Sterman, Nucl. Phys. **B250**, 199 (1985).
84. S. Catani, *et al.*, Nucl. Phys. **B407**, 3 (1993).
85. S. Fleming, arXiv:0907.3897 [hep-ph].
86. S. Catani, *et al.*, Phys. Lett. **B269**, 432 (1991).
87. N. Brown and W.J. Stirling, Phys. Lett. **B252**, 657 (1990).
88. W. Bartel, *et al.*, [JADE Collaboration], Z. Phys. **C33**, 23 (1986).
89. N. Kidonakis, G. Oderda, and G. Sterman, Nucl. Phys. **B531**, 365 (1998) [arXiv:hep-ph/9803241].
90. R. Bonciani *et al.*, Phys. Lett. **B575**, 268 (2003) [arXiv:hep-ph/0307035].
91. A. Banfi, G.P. Salam, and G. Zanderighi, JHEP **0503**, 073 (2005) [arXiv:hep-ph/0407286].
92. D. de Florian and M. Grazzini, Phys. Rev. Lett. **85**, 4678 (2000) [arXiv:hep-ph/0008152].
93. G. Bozzi *et al.*, Phys. Lett. **B564**, 65 (2003) [arXiv:hep-ph/0302104].
94. C. Balazs and C.P. Yuan, Phys. Rev. **D56**, 5558 (1997) [arXiv:hep-ph/9704258].
95. D. de Florian and M. Grazzini, Nucl. Phys. **B704**, 387 (2005) [arXiv:hep-ph/0407241].
96. S. Moch and P. Uwer, Phys. Rev. **D78**, 034003 (2008) [arXiv:0804.1476 [hep-ph]].
97. N. Kidonakis and R. Vogt, Phys. Rev. **D78**, 074005 (2008) [arXiv:0805.3844 [hep-ph]].
98. M. Beneke, P. Falgari, and C. Schwinn, arXiv:0907.1443 [hep-ph].
99. M. Czakon, A. Mitov, and G. Sterman, arXiv:0907.1790 [hep-ph].
100. A. Ferroglia *et al.*, arXiv:0907.4791 [hep-ph].
101. T. Becher and M.D. Schwartz, JHEP **0807**, 034 (2008) [arXiv:0803.0342 [hep-ph]].
102. S. Moch and A. Vogt, Phys. Lett. **B631**, 48 (2005) [arXiv:hep-ph/0508265].
103. E. Laenen and L. Magnea, Phys. Lett. **B632**, 270 (2006) [arXiv:hep-ph/0508284].
104. T. Sjostrand *et al.*, Comput. Phys. Commun. **135** 238, (2001) [arXiv:hep-ph/0010017].

105. T. Sjostrand, S. Mrenna, and P. Skands, JHEP **0605**, 026 (2006) [arXiv:hep-ph/0603175]; http://projects.hepforge.org/pythia6/.
106. T. Sjostrand, S. Mrenna, and P. Skands, Comput. Phys. Commun. **178** 852, (2008) [arXiv:0710.3820 [hep-ph]]; http://home.thep.lu.se/∼torbjorn/ Pythia.html.
107. B.R. Webber, Nucl. Phys. **B238**, 492 (1984).
108. G. Corcella *et al.*, JHEP **0101**, 010 (2001) [arXiv:hep-ph/0011363]; http://hepwww.rl.ac.uk/theory/seymour/herwig/.
109. M. Bahr *et al.*, Eur. Phys. J. **C58**, 639 (2008) [arXiv:0803.0883 [hep-ph]]; http://projects.hepforge.org/herwig/.
110. T. Gleisberg *et al.*, JHEP **0902**, 007 (2009) [arXiv:0811.4622 [hep-ph]]; http://projects.hepforge.org/sherpa/.
111. L. Lonnblad, Comput. Phys. Commun. **71** 15, (1992).
112. T. Sjostrand, arXiv:hep-ph/0611247.
113. B. Andersson *et al.*, Phys. Reports **97**, 31 (1983).
114. T. Sjostrand, Nucl. Phys. **B248**, 469 (1984).
115. S. Catani *et al.*, JHEP **0111**, 063 (2001) [arXiv:hep-ph/0109231].
116. J. Alwall *et al.*, Eur. Phys. J. **C53**, 473 (2008) [arXiv:0706.2569 [hep-ph]].
117. S. Frixione and B.R. Webber, JHEP **0206**, 029 (2002) [arXiv:hep-ph/0204244].
118. P. Nason, JHEP **0411**, 040 (2004) [arXiv:hep-ph/0409146].
119. M. Cacciari *et al.*, JHEP **0404**, 068 (2004) [arXiv:hep-ph/0303085].
120. M. Dasgupta and G.P. Salam, J. Phys. **G30**, R143 (2004) [arXiv:hep-ph/0312283].
121. S. Moretti, L. Lonnblad, and T. Sjostrand, JHEP **9808**, 001 (1998) [arXiv:hep-ph/9804296].
122. G.P. Salam, arXiv:0906.1833 [hep-ph].
123. S.D. Ellis *et al.*, Prog. in Part. Nucl. Phys. **60**, 484 (2008) [arXiv:0712.2447 [hep-ph]].
124. G.P. Salam and G. Soyez, JHEP **0705**, 086 (2007) [arXiv:0704.0292 [hep-ph]].
125. S. Catani *et al.*, Nucl. Phys. **B406**, 187 (1993).
126. S.D. Ellis and D.E. Soper, Phys. Rev. **D48**, 3160 (1993) [arXiv:hep-ph/9305266].
127. Y.L. Dokshitzer *et al.*, JHEP **9708**, 001 (1997) [arXiv:hep-ph/9707323].
128. M. Wobisch and T. Wengler, arXiv:hep-ph/9907280.
129. M. Cacciari, G.P. Salam, and G. Soyez, JHEP **0804**, 063 (2008) [arXiv:0802.1189 [hep-ph]].
130. M. Cacciari and G.P. Salam, Phys. Lett. **B641**, 57 (2006) [arXiv:hep-ph/0512210]; M. Cacciari, G.P. Salam, and G. Soyez, http://fastjet.fr/.
131. P.A. Delsart, K. Geerlins, and J. Huston, http://www.pa.msu.edu/∼huston/SpartyJet/SpartyJet.html.

132. S. Brandt *et al.*, Phys. Lett. **12**, 57 (1964).
133. E. Farhi, Phys. Rev. Lett. **39**, 1587 (1977).
134. O. Biebel, Phys. Reports **340**, 165 (2001).
135. S. Kluth, Rept. on Prog. in Phys. **69**, 1771 (2006) [arXiv:hep-ex/0603011].
136. A. Banfi, G.P. Salam, and G. Zanderighi, JHEP **0408**, 062 (2004) [arXiv:hep-ph/0407287].
137. D.E. Acosta *et al.*, [CDF Collaboration], Phys. Rev. **D71**, 112002 (2005) [arXiv:hep-ex/0505013].
138. T. Aaltonen *et al.*, [CDF Collaboration], Phys. Rev. **D78**, 072005 (2008) [arXiv:0806.1699 [hep-ex]].
139. C. Adloff *et al.*, [H1 Collaboration], Nucl. Phys. **B545**, 3 (1999) [arXiv:hep-ex/9901010].
140. S. Chekanov *et al.*, [ZEUS Collaboration], Nucl. Phys. **B700**, 3 (2004) [arXiv:hep-ex/0405065].
141. C. Glasman [H1 Collaboration and ZEUS Collaboration], Nucl. Phys. (Proc. Supp.) **191**, 121 (2009) [arXiv:0812.0757 [hep-ex]].
142. M. Martinez, arXiv:0905.2727 [hep-ex].
143. J.M. Campbell, J.W. Huston, and W.J. Stirling, Rept. on Prog. in Phys. **70**, 89 (2007) [arXiv:hep-ph/0611148].
144. C. Royon, arXiv:0811.1544 [hep-ex].
145. V.D. Elvira [D0 Collaboration and CDF Collaboration], arXiv:0808.0901 [hep-ex].
146. C. Glasman, arXiv:0810.3570 [hep-ex].
147. F.D. Aaron *et al.*, [H1 Collaboration], arXiv:0904.3870 [hep-ex].
148. F.D. Aaron *et al.*, [H1 Collaboration], Eur. Phys. J. **C54**, 389 (2008) [arXiv:0711.2606 [hep-ex]].
149. S. Chekanov *et al.*, [ZEUS Collaboration], Eur. Phys. J. **C52**, 515 (2007) [arXiv:0707.3093 [hep-ex]].
150. S. Chekanov *et al.*, [ZEUS Collaboration], Phys. Rev. **D78**, 032004 (2008) [arXiv:0802.3955 [hep-ex]].
151. S. Chekanov *et al.*, [ZEUS Collaboration], Nucl. Phys. **B792**, 1 (2008) [arXiv:0707.3749 [hep-ex]].
152. S. Chekanov *et al.*, [ZEUS Collaboration], Phys. Rev. **D76**, 072011 (2007) [arXiv:0706.3809 [hep-ex]].
153. A. Aktas *et al.*, [H1 Collaboration], Phys. Lett. **B639**, 21 (2006) [arXiv:hep-ex/0603014].
154. A. Abulencia *et al.*, [CDF - Run II Collaboration], Phys. Rev. **D75**, 092006 (2007) [Erratum-ibid. 119901] [arXiv:hep-ex/0701051].
155. V.M. Abazov *et al.*, [D0 Collaboration], Phys. Rev. Lett. **101**, 062001 (2008) [arXiv:0802.2400 [hep-ex]].
156. T. Kluge, K. Rabbertz, and M. Wobisch, arXiv:hep-ph/0609285.
157. K. Rabbertz, private communication, Aug 2009.
158. T. Aaltonen *et al.*, [CDF Collaboration], Phys. Rev. **D79**, 112002 (2009) [arXiv:0812.4036 [hep-ex]].

159. V.M. Abazov *et al.*, [D0 Collaboration], arXiv:0906.4819 [hep-ex], submitted to Phys. Rev. Lett.
160. V.M. Abazov *et al.*, [D0 Collaboration], Phys. Rev. Lett. **94**, 221801 (2005) [arXiv:hep-ex/0409040].
161. V.M. Abazov *et al.*, [D0 Collaboration], Phys. Rev. Lett. **678**, 45 (2009) [arXiv:0903.1748 [hep-ex]].
162. V.M. Abazov *et al.*, [D0 Collaboration], Phys. Lett. **B669**, 278 (2008) [arXiv:0808.1296 [hep-ex]].
163. T. Aaltonen *et al.*, [CDF - Run II Collaboration], Phys. Rev. Lett. **100**, 102001 (2008) [arXiv:0711.3717 [hep-ex]].
164. T. Aaltonen *et al.*, [CDF Collaboration], Phys. Rev. **D77**, 011108 (2008) [arXiv:0711.4044 [hep-ex]].
165. CDF Collaboration, public note 8418, July 2006; see also http://www-cdf.fnal.gov/physics/new/qcd/abstracts/bjet_05.html.
166. V.M. Abazov *et al.*, [D0 Collaboration], Phys. Rev. Lett. **102**, 192002 (2009) [arXiv:0901.0739 [hep-ex]].
167. V.M. Abazov *et al.*, [D0 Collaboration], Phys. Lett. **B666**, 23 (2008) [arXiv:0803.2259 [hep-ex]].
168. T. Aaltonen *et al.*, [CDF Collaboration], Phys. Rev. Lett. **100**, 091803 (2008) [arXiv:0711.2901 [hep-ex]].
169. A. Abulencia *et al.*, [CDF Collaboration], Phys. Rev. **D74**, 032008 (2006) [arXiv:hep-ex/0605099].
170. T. Aaltonen *et al.*, [CDF collaboration], arXiv:0812.4458 [hep-ex], submitted to Phys. Rev. D..
171. S. Bethke, Prog. in Part. Nucl. Phys. **58**, 351 (2007) [arXiv:hep-ex/0606035].
172. S. Bethke, arXiv:0908.1135 [hep-ph].
173. S. Bethke, J. Phys. **G26**, R27 (2000) [arXiv:hep-ex/0004021].
174. M. Beneke and M. Jamin, JHEP **0809**, 044 (2008) [arXiv:0806.3156 [hep-ph]].
175. M. Davier *et al.*, Eur. Phys. J. **C56**, 305 (2008) [arXiv:0803.0979 [hep-ph]].
176. K. Maltman and T. Yavin, Phys. Rev. **D78**, 094020 (2008) [arXiv:0807.0650 [hep-ph]].
177. S. Menke, arXiv:0904.1796 [hep-ph].
178. S. Narison, Phys. Lett. **B673**, 30 (2009) [arXiv:0901.3823 [hep-ph]].
179. I. Caprini and J. Fischer, arXiv:0906.5211 [hep-ph], acc. by Eur. Phys. J. C..
180. H. Flacher *et al.*, Eur. Phys. J. **C60**, 543 (2009) [arXiv:0811.0009 [hep-ph]].
181. J. Blumlein, H. Bottcher, and A. Guffanti, Nucl. Phys. **B774**, 182 (2007) [arXiv:hep-ph/0607200].
182. G. Dissertori *et al.*, JHEP **0908**, 036 (2009) [arXiv:0906.3436 [hep-ph]].
183. S. Bethke *et al.*, [JADE Collaboration], arXiv:0810.1389 [hep-ex].
184. C. Glasman [H1 Collaboration and ZEUS Collaboration], J. Phys. Conf. Ser. **110** 022013 (2008) [arXiv:0709.4426 [hep-ex]].

185. N. Brambilla *et al.*, Phys. Rev. **D75**, 074014 (2007) [arXiv:hep-ph/0702079].
186. C.T.H. Davies *et al.*, [HPQCD Collaboration], Phys. Rev. **D78**, 114507 (2008) [arXiv:0807.1687 [hep-lat]].
187. C.T.H. Davies *et al.*, [HPQCD Collaboration, UKQCD Collaboration, and MILC Collaboration], Phys. Rev. Lett. **92**, 022001 (2004) [arXiv:hep-lat/0304004].
188. K. Maltman, *et al.*, Phys. Rev. **D78**, 114504 (2008) [arXiv:0807.2020 [hep-lat]].
189. S. Aoki, *et al.*, [PACS-CS Collaboration], arXiv:0906.3906 [hep-lat].
190. M. Schmelling, Phys. Scripta **51**, 676 (1995).